Jet Sets

G.P. WILLIAMS

Geophysical Fluid Dynamics Laboratory/NOAA, Princeton University, Princeton, New Jersey, USA

(Manuscript received 26 August 2002, in revised form 17 January 2003)

Abstract

To broaden the range of known circulations and to test existing theory, a variety of issues are examined concerning the dynamics of flows in thick, thin, and transitional atmospheric layers. The circulations are produced numerically using a primitive equation model subject to simple heating functions. To confine the motions to a thin upper layer, the heating is chosen to produce a flow with either an exponential (EXP) vertical structure, or one that is linear (LIN) aloft while vanishing below. Five sets of solutions are created to define the terrestrial and jovian axisymmetric states, some basic terrestrial states, and the transitional jovian states for the two structures.

The axisymmetric cases examine how the surface drag, static stability, rotation rate, and layer thickness influence the flow character. The standard theory is extended to allow for a weaker drag and the solutions confirm that at lower rates the Hadley cells become wider, and the thermal fronts sharper and double. In the absence of any drag, the cells disappear and a thermal wind prevails globally. But in the absence of a background static stability, the cells become more intense and create their own stable temperature field. For normal parameter values, the Hadley cells adhere to the theoretical form as the rotation rate increases, except when their width falls below 3° of latitude. Furthermore, when the heated layer is thin and the jets are confined aloft, the cells develop vertically bimodal amplitudes, while remaining deep and exhibiting the usual widths.

The basic 3-D terrestrial cases examine the role of the heating rate, static stability, surface drag, and rotation rate on the flow character. The mean jets exist within a limited latitudinal range, with their location being as much dependent on the heating amplitude as on the heating distribution. When the background static stability is absent, the standard circulation theory becomes less valid as the cells and baroclinic instability become more intense and act together to stabilize low and middle latitudes. However, when the drag is reduced, the baroclinic instability becomes much weaker and confined to lower levels because of suppression by the jet's stronger barotropic component. Other forms of baroclinic instability can be produced by creating double-jet flows, either by increasing the rotation rate or by adding an extra source of baroclinicity in low latitudes.

The transitional jovian cases examine how the multiple jets behave as the active layer is varied between thick and thin for the LIN and EXP structures. In all cases, the jet widths remain constant with latitude, but their amplitudes vary, peaking either in low or middle latitudes depending on how the baroclinicity is distributed. An extra baroclinicity in low latitudes produces a jet whose barotropic instability can drive an equatorial superrotation, regardless of layer thickness. The eddy-driven jets have a similar dynamics for all layer thicknesses but, unlike the steady LIN jets, the EXP jets also migrate equatorward and, on rare occasions, poleward.

Corresponding author: G.P. Williams, Geophysical Fluid Dynamics Laboratory/NOAA, Princeton University, P.O. Box 308, Princeton, NJ 08542-0308, USA.
E-mail: gw@gfdl.noaa.gov and /www.gfdl.noaa.gov/~gw/.
© 2003, Meteorological Society of Japan

1. Introduction

In previous papers (Williams 1988, 2003a), the dynamical range of global circulations was examined for both the terrestrial, and jovian systems, by varying the basic parameters of

primitive equation models. The jovian system was assumed to be equivalent to a larger, faster-rotating Earth, with baroclinically driven flows confined to a thin upper layer. We now examine whether these two systems represent two separate classes of flow, or whether they just describe the limits to a continuum of circulations. To do this, the transition between the thin and thick flows is evaluated using both the terrestrial and jovian parameters for both the axisymmetric and 3-D states, to see if the dynamics changes in any fundamental way as the thickness of the active layer changes.[1] The resulting solutions also broaden the range of basic circulation forms that can be used for testing, or extending existing theories.

Essentially, the previous studies show that the terrestrial models can have one or more jets per hemisphere, depending on the rotation rate, and that the jovian models can have multiple jets driven by baroclinic instabilities in thin layers. Furthermore, there appear to be two classes of jovian jet, depending on the vertical structure. Steady jets occur when the heating produces a flow that has a linear (LIN) structure in the active layer, but nothing in the sublayer, while migrating jets occur when the heating produces a flow with an exponential (EXP) structure having a high confinement rate—see Fig. 1. The EXP jets migrate slowly equatorward and regenerate in high latitudes. In addition, equatorial jets can be generated by barotropic instabilities in either system when there is sufficient baroclinicity in low latitudes to create a tropical jet.

The present study is partly based on a three-part series of calculations using a primitive equation model that examine dynamical processes thought to be relevant to the global circulations of the jovian atmospheres. In Part I (Williams 1996), zonal jets are seen to be capable of generating and coexisting with planetary scale vortices (resembling the Great Red Spot), that are absolutely stable in low latitudes when all of the horizontal motions are limited to a thin upper layer by confined heating forms,

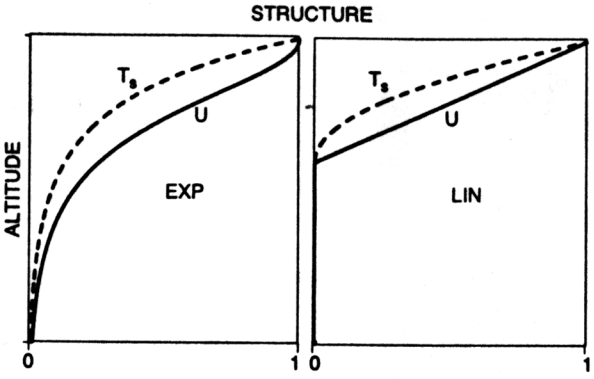

Fig. 1. Schematic diagram of the vertical form of the static stability and zonal flow produced by the LIN and EXP heating structures, shown for the upper regions only.

with the EXP and LIN structures. The extension of the vortex modeling to a wider range of latitudes, in Part II (Williams 2002), indicates that the EXP and LIN structures could prevail globally in the jovian system. The vortices are generated by the long-wave baroclinic instability of baroclinic easterly jets, and their relation to the long-wave solitary Rossby waves provides, via the propagation rate, a deformation radius of about 1000 km as an upper limit for the size of the eddies that sustain the jets. In addition, the creation of steady vortex configurations, using a Newtonian heating function, provides an estimate of about 300 days as a representative timescale for the thermal processes. These space and time scales are also used for the jovian aspects of the present study.

Further calculations, in Part III (Williams 2003a), show that the baroclinic instabilities needed to produce the small eddies, and energize their cascade into multiple jets, can occur in both the thin EXP and LIN systems. However, the two structures have some different small-scale properties, particularly as regards the latitudinal eddy heat fluxes and jet migration, even though they allow a similar large-scale vortex behavior. In addition, the instabilities can be extended into low latitudes where, in turn, they can lead to the formation of superrotating westerlies at the equator.

Now, to map out the connections between the thin and thick systems, five related sets of solutions are developed and described—in figure

1 By *thick* or *thin* systems, we mean layers whose motions either extend over the whole depth or are confined to an upper region overlying a deeper sublayer.

groups A–E—starting with the axisymmetric states that underlie the 3-D circulations that follow. For the axisymmetric states, the terrestrial system is used to examine the influence of some basic parameters on the circulation form. Then the jovian 2-D system is used to examine the transitions from high to low rotation rates, and from thick to thin layers. For the 3-D states, the terrestrial system is used to examine the influence of certain basic parameters on the circulation elements, particularly on the form of the baroclinic instabilities. Then the jovian 3-D system is evaluated using both the LIN and EXP structures to define the transitions that occur in the multi-jet flows as the heated layer goes from thick to thin. Some of the cases raise questions, such as the following, that require an extension of circulation theory to resolve.

For example, for the axisymmetric state, it would be useful to understand what happens to the circulation when the drag or the static stability are so weak, or the rotation rate is so high that the theoretical constraints of standard theory no longer hold. How do cells and jets form when there is no background static stability? Can the numerical model handle a drag-free system? Does the circulation develop any unpredicted features at other rotation rates or at other thicknesses, features not seen in the standard calculations? In other words, how representative is existing theory?

Turning to the terrestrial 3-D system, we would also like to know what happens to the baroclinic instability when the drag, or the background static stability are weak. Such 3-D and axisymmetric solutions may be relevant to the neutrally-stable terrestrial tropics and the low-drag jovian atmospheres. Then, as a prelude to understanding the equatorial superrotation, it would be useful to know what factors determine the mean jet location. What role does the heating amplitude play in this? When do double jets form and contain a low-latitude component that can generate an equatorial westerly? Such solutions should also help define the glacial climate associated with the equatorial superrotation discussed in Williams (2003b).

For the jovian system with the LIN and EXP structures, we primarily need to know whether the character of the circulation changes as the depth of the active layer changes from thin to thick. Do baroclinic instabilities always develop in confined layers? Do the jets migrate at all confinement rates in the EXP system and, if so, is the migration always equatorward or can it also be poleward? Such solutions are needed to help isolate the vertical structure, and parametric sensitivity, of the jovian circulations.

The presentation begins in section 2 with a description of the basic model, the parameters, and the design of the heating distributions. This is followed by a brief review of those theories that help in designing the calculations and in understanding the solutions. Section 3 then extends axisymmetric theory, and describes the various axisymmetric states in the terrestrial and jovian sets. Sections 4–6 do the same for the basic 3-D terrestrial, jovian LIN, and jovian EXP sets, respectively. The questions that arise, and any theories that are pertinent, are discussed in the individual sections. Section 7 summarizes the results and their implications.

2. Numerical model

2.1 System of equations

The numerical studies use the primitive equations of motion with a Boussinesq equation of state, solved for a regional channel on a sphere. This model provides an adequate representation of the basic dynamical mechanisms under consideration and can be applied to either an ocean or an atmosphere provided that, for the latter, the variables are mapped from geopotential to pressure coordinates and reinterpreted appropriately, as described by Salmon (1998, p. 102).

The primitive equation model for a thin hydrostatic fluid is specified by the zonal, meridional, and vertical velocity components u, v, and w, and by the pressure, density, and temperature fields p, ρ, and T. The standard equations include horizontal and vertical diffusion terms, as well as a heating function, Q, and a convective adjustment. They are written in spherical coordinates as

$$u_t + L(u) - v(f + mu) = \frac{-1}{ac\rho_0} p_\lambda + F^u, \qquad (1)$$

$$v_t + L(v) + u(f + mu) = \frac{-1}{a\rho_0} p_\phi + F^v, \qquad (2)$$

$$T_t + L(T) = Q + F^T, \tag{3}$$

$$p_z = -g\rho, \quad \rho = \rho_0[1 - \alpha(T - T_0)], \tag{4}$$

where, for $q \equiv u$, v, or T, the nonlinear advection forms are

$$L(q) = \frac{1}{ac}[(uq)_\lambda + (cvq)_\phi] + (wq)_z, \tag{5}$$

with the identity $L(1) = 0$ for the mass conservation defining the w field.

The diffusion terms representing the grid scale eddies use simple biharmonic and second-derivative forms in the horizontal and vertical, respectively:

$$F^{(u,v,T)} = \nu_4 \nabla^4 (u, v, T) + \nu_2 \left(u, v, \frac{T}{\gamma}\right)_{zz}, \tag{6}$$

where the coefficient ν_4 is negative and the parameter γ (= 0 or 1) indicates that convective adjustment is implemented when the fluid is vertically unstable, and where $\nabla^2 q$ is the Laplacian operator.

The variables λ, ϕ, z represent the longitude, latitude, and height; g is the gravity; Ω and a are the planetary angular velocity and radius; $f = 2\Omega \sin\phi$ and $\beta = 2\Omega a^{-1} \cos\phi$ are the Coriolis parameters; $m = (1/a) \tan\phi$ and $c = \cos\phi$ are map parameters; ρ_0 and T_0 denote two reference values; T_s and α are the background hydrostatic temperature and the Boussinesq coefficient; while $B = \alpha g(dT/dz)$ defines the Brunt-Väisälä stability parameter. Finally, the parameter Ω^* refers to the rotation rate normalized by the standard value for the planet under discussion, and Ψ defines the meridional streamfunction.

The equations are solved using the finite difference methods documented in Part I, following the classical method of Bryan (1969). These involve a leapfrog time differencing and a centered spatial differencing on the so-called Arakawa B grid. The computational domain consists of a southern hemisphere channel with periodic boundary conditions in longitude, symmetry conditions at the northern boundary on the equator, together with a no-slip, no-flux condition on the southern wall. In the vertical, both surfaces are taken to be horizontal rigid lids with free-slip, no-flux conditions at $z = 0$ and H, where H is the fluid thickness. Near the lower surface, a linear drag with a timescale τ_D helps equilibrate some flows.

2.2 *Parameter values*

For the terrestrial (thick layer) cases, the basic parameters are: $a = 6400$ km, $g = 9.8$ m s^{-2}, $\Omega = 7.3 \times 10^{-5}$ s^{-1}, $H = 8$ km, $\nu_4 = -10^{15}$ m^4 s^{-1}, and $\nu_2 = 1$ m^2 s^{-1}; for a domain extending over 180° in longitude and 70° in latitude, and resolved by grids with $\Delta\lambda = 3°$, $\Delta\phi = 1°$, $\Delta z = H/20$, and $\Delta t = (1/100)$ day. The Boussinesq coefficient is set at $\alpha = 0.003°\text{C}^{-1}$. Deviations from these values are listed in the various Tables for the heating parameters.

The jovian (thin and thick layer) cases use parameter values that are thought to be appropriate for Jupiter's atmosphere, values that produce zonal jets with amplitudes, scales, and form comparable to those observed at cloud level. The planetary parameters, $a = 71300$ km, $\Omega = 1.76 \times 10^{-4}$ s^{-1}, and $g = 26$ m s^{-2} remain fixed. For evaluation purposes, H is nominally set at 15000 km but, as discussed in Part II, it can be reduced by a factor of 10 or more and all solutions can be rescaled in the vertical without altering their form, provided that the temperature gradients are increased by a corresponding factor to maintain identical winds. The value of $\alpha = 0.005°\text{C}^{-1}$ is arbitrary, and the diffusion coefficients are set close to $\nu_4 = -10^{17}$ m^4 s^{-1} and $\nu_2 = 10^4$ m^2 s^{-1}, to represent eddies that are larger than their terrestrial counterparts.

The jovian domain generally ranges over 60° of longitude and 70° of latitude, with $\Delta\lambda = 1°$ and $\Delta\phi = 1°$ forming the standard grid spacing, and with $\Delta t = (1/100)$ day being a typical timestep.[2] A uniform vertical grid is used for systems that are thick or moderately thin. For the EXP cases whose structure goes as $\exp(Nz')$, the vertical grid Δz varies exponentially in its spacing when $N > 5$; for example, as $\exp(7z')$ when the confinement rate N equals 200, to put more than half the grid points in the active layer, where $z' = z/H$. Likewise, in the very thin LIN cases, a simple split grid with $\Delta z = [\Delta z_1, \Delta z_2] = [0.05, 0.95]2H/KZ$, puts one half of the grid points, the thinly spaced ones, in an upper layer of thickness $h_1 = H/20$ that contains the main motion, and the other half, the thickly spaced ones, in the sublayer; where the number of gridpoints KZ usually equals 20.

2 A day equals 86400 seconds in this paper.

In presenting the solutions, the figures use solid contour lines to plot values greater than, or equal to zero, while dashed lines denote negative values. For the time-mean eddy transports, evaluated using fields sampled at one-day intervals, the zero-value contours are omitted from the plots for greater clarity. The temperature field also omits the constant T_0 value. Altitude is measured in kilometers in the vertical cross sections. Indices are used to refer to phenomena by zone, starting at the equator, so that W_0 refers to the superrotating westerly, followed by W_1 for the low-latitude westerly and, thereafter, by W_i $(i = 2, 3, \ldots)$ for the numerous midlatitude jets. For simplicity in discussing the solutions, the negative sign of the southern hemisphere latitudes is ignored.

2.3 *Heating functions*

All flows are developed from rest and maintained by a Newtonian heating function of the form

$$Q(\phi, z, t) = \frac{T_r - T}{\tau}, \tag{7}$$

where the heating rate is proportional to the difference between the fluid temperature and a specified radiative-convective equilibrium temperature $T_r(\phi, z)$. The radiative-convective damping time $\tau(\phi, z)$ is set to constant values. After spinning up and perturbing the axisymmetric state, the flow is maintained with $\tau = 20$ and 300 days for the terrestrial and jovian cases, respectively.

The following form is used to heat the active layer, thick or thin:

$$T_r = \Delta T \cdot P(\phi) \cdot S_1(z) + \delta T \cdot S_2(z), \tag{8}$$

where the structure varies as $S_1 = 1$ and $S_2 = z'$ for Earth. The amplitudes ΔT and δT set the baroclinicity and static stability rates, where $T_s = \delta T \cdot S_2(z)$. For the jovian cases, the refined form $S_1 = (d/dz)[\mathrm{sech}(Nz')]$ in the EXP system produces $u(z)$ profiles that are exponential at depth, while having a vanishing shear at the upper surface, as in Fig. 1. The structure of the hydrostatic temperature, $S_2 = \exp(Nz')$, remains independent of latitude. For the LIN system, the structures are defined, as in Part I, by the split functions $S = C[1, 0]$ and $T_s = \delta T \cdot C[z_c^2, 0]$, where C symbolizes confinement, and where the first factors define the distributions used to produce a linear $u(z)$ and a linear $B_s(z)$ in an upper region of depth $h \approx 0.7h_1$, with $z_c = 1 - |z/h|$ over $|z| \le h$. The second factors define the abyssal distributions. The upper region extends over about 7 gridpoints when $KZ = 20$, so the main motions always lie well within the highly resolved layer and experience no computational problems at the Δz_1 to Δz_2 interface.[3] The ratio $h' = h/H$ defines a confinement parameter for the LIN system.

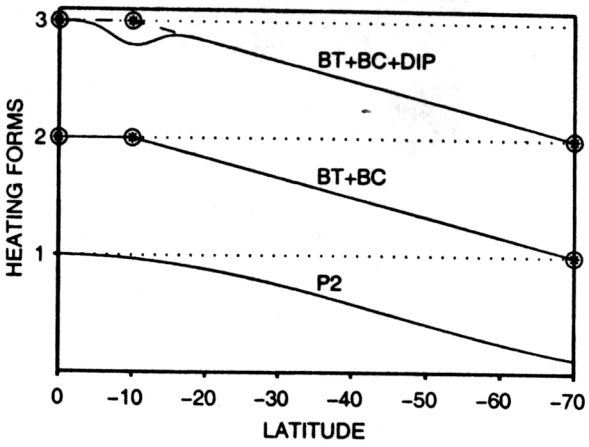

Fig. 2. Schematic diagram showing the latitudinal heating distributions used in the calculations. The profiles are referred to in the text as the P_2, P_{BT+BC}, and P_{DIP} forms, where BT, BC, and DIP indicate barotropic, baroclinic, and Gaussian components.

To provide a global baroclinicity, the latitudinal heating distribution $P(\phi)$ is first based on the second Legendre polynomial and set equal to $\cos^2\phi$—denoted as $P_2(\phi)$—where only positive values are used so as to avoid cooling and inducing large-scale convection in a confined layer—see Fig. 2. As the P_2 distribution is not universal enough to yield the full range of circulations, the form of $P(\phi)$ is varied by introducing separate barotropic and baroclinic zones in some cases. Thus to examine the influence of a barotropic (BT) zone at the equator, its extent into the tropics is varied by replacing P_2 by P_{BT+BC}, a combination of a tropical BT

3 This was verified by comparison with calculations using uniform or exponential grids.

zone and a midlatitude baroclinic (BC) zone.[4] The $P(\phi)$ distribution also has a form, P_{DIP}, which is equivalent to P_{BT+BC} with a Gaussian cooling component added (at the latitude where the BT and BC zones meet) to boost the baroclinicity in low latitudes. All $P(\phi)$ profiles are normalized so as to vary between one and zero. Heating profiles resembling P_{DIP} have been used in dry Earth models to allow implicitly for the intense heating gradient produced by condensation at the equator (Smagorinsky 1963, Fig. A5).

These heating forms are used to generate five sets of solutions that are primarily developed to examine the types of circulation that can occur in axisymmetric and 3-D systems over a range of atmospheric thicknesses and basic parameters, particularly the static stability, rotation rate, and surface drag. Such calculations are needed to broaden the base from which to extrapolate from Earth to the other planets, where the values of some basic parameters are unknown and where the vertical structure and underlying dynamics are uncertain. They are also needed to test the range of validity of the theories developed for the existing terrestrial state.

2.4 *Theoretical background*

The present understanding of axisymmetric circulations comes from variations on the classical balance theory of Schneider (1977) and Held and Hou (1980), as discussed below in section 3.1. On the other hand, the existence of multiple 3-D jets is usually explained theoretically in terms of the barotropic and baroclinic modes of energy and enstrophy cascade associated with the various forms of β turbulence, as described by Rhines (1975, 1977, 1994). Consequently, the generation and persistence of multiple jets have been explored numerically using a variety of atmospheric, oceanic, and planetary models. The models range from barotropic spheres (Williams 1978; Huang and Robinson 1998; Huang et al. 2001), to quasi-geostrophic (QG) beta planes (Williams 1979a,b; Panetta 1993; Vallis and Maltrud 1993; Treguier and Panetta 1994; Lee 1997), to shallow water spheres (Williams and Wilson 1988; Cho and Polvani 1996), to primitive equation general circulation models (GCMs) (Williams 1988).

For thin layers, as for thick, linear baroclinic instability theory can be used to explain eddy origin and scale, and nonlinear theory can be used to explain eddy evolution and fluxes. In the classical ocean study of Gill et al. (1974) for exponentially structured flows, the latitudinally-independent, quasi-geostrophic flows on a beta plane can be unstable if the potential vorticity (q) gradient

$$q_y = \beta + f\left(\frac{\rho_y}{\rho_z}\right)_z = \beta - \left(\frac{u_z}{s}\right)_z, \tag{9}$$

changes sign internally or opposes the sign of u_z at the upper boundary, where $s = B/f^2$ and y is the meridional coordinate. Instability is primarily determined by the slope of the isopycnals. When the slope is uniform, only easterly flows are unstable. To destabilize the westerly flow produced by the standard atmospheric heating requires that the symmetry between the $u(z)$ and $B(z)$ distributions in exponential systems be broken. Asymmetries occur in the numerical EXP solutions where the static stabilities have a strong jet-related component B_j, that tends to dominate the background component B_s aloft.

Furthermore, the results given by the advective model of baroclinic instability, as derived by Fjortoft (1951) and evaluated for arbitrary $u(z)$ profiles by Wiin-Nielsen (1967), apply to both the LIN and EXP structures. The vertical heat transport term, Bw, is assumed to be negligible in this model, which makes it useful for understanding flows that may have a non-QG balance or may have a complex or negligible $B(z)$. The analysis of Wiin-Nielsen for arbitrary $u(z)$ profiles shows that disturbances of the form $\exp[ik(x-ct)]$ have a phase speed given by

$$c = \left(I_1 - \frac{c_r}{2}\right) \pm \left(I_1^2 - I_2 + \frac{c_r^2}{4}\right)^{1/2}, \tag{10}$$

where $c_r = \beta/k^2$, $I_1 = \int_0^1 u\,dz'$, $I_2 = \int_0^1 u^2\,dz'$. Instability occurs according to Schwartz's inequality when $I_2 - I_1^2 > c_r^2/4$, which implies that westerlies are unstable at scales $L < L_\beta(2/N)^{1/4}$ and $L < L_\beta(2h/H)^{1/2}$ in the EXP and LIN systems, respectively, where $L_\beta = (U/\beta)^{1/2}$ for the velocity scale U. For the nu-

4 By *barotropic* or *baroclinic* zones, we mean regions with latitudinally uniform or latitudinally linear heating distributions, respectively.

merical cases with $N \sim 200$ or $h' \sim 1/20$, the cutoff occurs at $L \sim L_\beta/4$. Similar criteria for the instability of thin-layer westerlies are given by Killworth (1980, section 9b) and Benilov (1995, section 5).

The nonlinear baroclinic instability theories that follow eddy development through cycles of growth and decay, and help explain eddy evolution and fluxes in Earth's atmosphere, appear to be relevant to thin layers also. Detailed analyses of such "eddy cycles" indicate that, for a specified zonal flow, linear theory applies initially, with the eddy energy growing at all heights but transporting heat mainly at lower levels (Simmons and Hoskins 1978; Edmon et al. 1980). The upper level eddies, fed by upward wave radiation, generate planetary waves that propagate to other latitudes. These waves produce a large momentum flux that either traverses poleward, as in the standard terrestrial case, or converges on the jet cores, as in terrestrial models with higher rotation rates, Williams (1988). The dynamics of various forms of equatorial superrotation are discussed in detail by Suarez and Duffy (1992), Saravanan (1993), and Williams (2003b).

3. Axisymmetric states

The theory for axisymmetric circulations that is pertinent to the present study has been developed by Held and Hou (1980) and by Satoh (1994). Most other contributions have been concerned with trying to extend the theory to deal with off-equator heating peaks, a subject that is not considered here. Our concern is with examining what happens when some of the basic theoretical constraints are pushed or violated. In particular, we first examine the effect of drag on the circulation as this factor is generally weak in the thinner states to be examined later. Then we examine the circulations that form in the limit of zero static stability, high rotation rate, and zero drag. Finally, for variety, the jovian parameters are used when examining the full rotational range of axisymmetric circulations, as well as the vertically confined forms.

3.1 Theory

A simple model of the axisymmetric circulation that allows for a more general surface condition can be constructed by combining the theories of Satoh (1994) and Held and Hou (1980) to give a more general estimate for the width, ϕ_H, of the Hadley cell. For tractability, the upward flow of the Hadley circulation is assumed to be concentrated near the equator, while a near-uniform downflow extends to ϕ_H. Then, for simplicity, the small angle approximation is made for quantities near the equator. Thus, on integrating the mass conservation equation, the poleward mass flux V can be defined by the simple form

$$V(\phi) = Ma(\phi_H - \phi), \tag{11}$$

where the downward mass flux per unit area, M, is assumed to be almost constant from the equator to ϕ_H.[5]

Next, on assuming that the angular momentum is conserved in the top layer, the zonal wind in that layer may be written as

$$u_T(\phi) = a\Omega(\phi^2 - \phi_T^2), \tag{12}$$

where ϕ_T is the latitude at which the zonal flow vanishes. Then integrating the angular momentum equation over all levels gives

$$\frac{\partial}{\partial\phi}[V(u_T - u_B)] = -aC_D u_B, \tag{13}$$

where u_B is the zonal flow in the bottom layer, and C_D is a linear drag coefficient. Substituting (11) and (12) into (13) and integrating gives the value of u_B as

$$u_B(\phi) = a\Omega\phi_H^2\left[\frac{3}{C+3}\left(1-\frac{\phi}{\phi_H}\right)^2 - \frac{4}{C+2} \times \left(1-\frac{\phi}{\phi_H}\right) + \frac{1}{C+1}\left(1-\frac{\phi_T^2}{\phi_H^2}\right)\right], \tag{14}$$

where $C = C_D/M$.

On further assuming that the angular momentum is conserved in the upward branch of the cell at the equator, the identity

$$u_B(0) = u_T(0), \tag{15}$$

when combined with (12) and (14), gives the latitudes at which the zonal flow vanishes at the top and bottom:

5 We could assume a form, $V(\phi) = Ma\phi(\phi_H - \phi)$, that is in closer agreement with the numerical solutions but this results in equations that lack a simple analytical solution.

$$\phi_T = \left[\frac{2}{(C+2)(C+3)}\right]^{1/2}\phi_H, \tag{16}$$

$$\phi_B = \left[\frac{C+(C^2+6C+12)^{1/2}}{3(C+2)}\right]\phi_H. \tag{17}$$

In the strong-drag limit, $C \gg 1$, these give $\phi_T \approx 0$ and $\phi_B = (2/3)\phi_H$, while in the weak-drag limit, $C \ll 1$, they give $\phi_T = \phi_B = (1/\sqrt{3})\phi_H$.

The above velocity factors are all as derived by Satoh (1994) for a model driven by a heating with a fixed surface temperature. But we now deviate from that analysis and apply the velocity factors to the thermal criteria chosen by Held and Hou (1980) for a model driven by a Newtonian heating function that adjusts to an internal temperature field. Thus, on assuming a balanced zonal wind, the thermal wind equation integrated over height gives

$$\frac{\partial \bar{T}}{\partial \phi} = -2\left(\frac{a\Omega}{\alpha g H}\right)\phi[u_T - u_B], \tag{18}$$

where the overbar denotes a vertical average. Further integrations give the average radiative temperature as

$$\bar{T}_r = \bar{T}_r(0) - \Delta T \phi^2, \tag{19}$$

and the conservation of heat as

$$\int_0^{\phi_H} (\bar{T} - \bar{T}_r)\, d\phi = 0, \tag{20}$$

plus

$$\bar{T}(\phi_H) = \bar{T}_r(\phi_H), \tag{21}$$

for the boundary condition.

Finally, on substituting for u_T and u_B in (18) and integrating subject to the conditions (19)–(21), we get an expression for the width of the Hadley cell

$$\phi_H^2\left[1 - \frac{(C+12)}{2(C+3)(C+2)}\right] = \frac{5}{3}R, \tag{22}$$

where R defines the thermal Rossby number as

$$R = \frac{\alpha g H \Delta T}{a^2\Omega^2}. \tag{23}$$

In the strong-drag limit this width matches the value derived by Held and Hou (1980).

3.2 *Drag variants*

Consider now the first three numerical solutions for the terrestrial axisymmetric system which examine the effect of the surface drag on the circulation, cases EA1–EA3 in Fig. A1 and Table A1. The EA1 case represents the control or reference state, and resembles the low-viscosity solutions of Held and Hou (1980). The sloping Hadley cell extends from 15° at the ground to 25° aloft, and is accompanied by a weak Ferrel cell. The zonal flow has two components: the angular momentum conserving wind U_A in $\phi < \phi_H$, and the radiative thermal wind U_R in $\phi > \phi_H$. The two components merge in a nonlinear manner not covered by the theory and produce a second jet at 36°. The strong-drag limit of (16), (17) and (22) holds with $\phi_T \approx 0$ and $\phi_B = (2/3)\phi_H = 16°$ when $\phi_H = 24°$. These values require a drag factor of $C \leq 8$ when $R = 0.1$.

The EA2 case shows what happens when the drag is reduced by an order of magnitude. The zonal flow now has a strong barotropic component, plus two jet peaks separated by a sharp shear, and easterlies that occupy latitudes equatorward of 16°. A strong thermal front separates the two wind components at the boundary of the Hadley cell at 32°. The Hadley cell clearly increases its width as the drag weakens, and is in agreement with (22) if $C = 1.5$ and $R = 0.1$.

Reducing the drag to very weak levels by setting $\tau_D = 100$ days produces the EA3 flow with a predominant barotropic component, even though the two-component balance between the U_A and U_R winds still exists. For this case, the ΔT heating rate has been reduced to keep the winds at reasonable values. Both jet peaks now develop strong shear layers in two thermal fronts, at 43° and 53°. Easterlies form in low latitudes and also in the merging zone at 45°. Although the merging of the U_A and U_R winds is highly nonlinear, the basic theory seems to retain some validity, even at very weak drag rates. The extent of the main EA3 jet is consistent with the weak-drag limit of (16), (17) and (22), for which $\phi_T = \phi_B = (1/\sqrt{3})\phi_H = 22°$ and $\phi_H = 43°$, when $C = 0.16$ and $R = 0.035$.

Overall, the values $C = (8, 1.5, 0.16)$ deduced for the three cases correspond reasonably well, considering the simplifications, with the estimates based on the maximum streamfunction: $C = \Delta z/(M\tau_D) = (20, 0.8, 0.06)$, where $M = a^{-1}\Psi_{max}$. Finally, note that (22) gives $\phi_H = \infty$

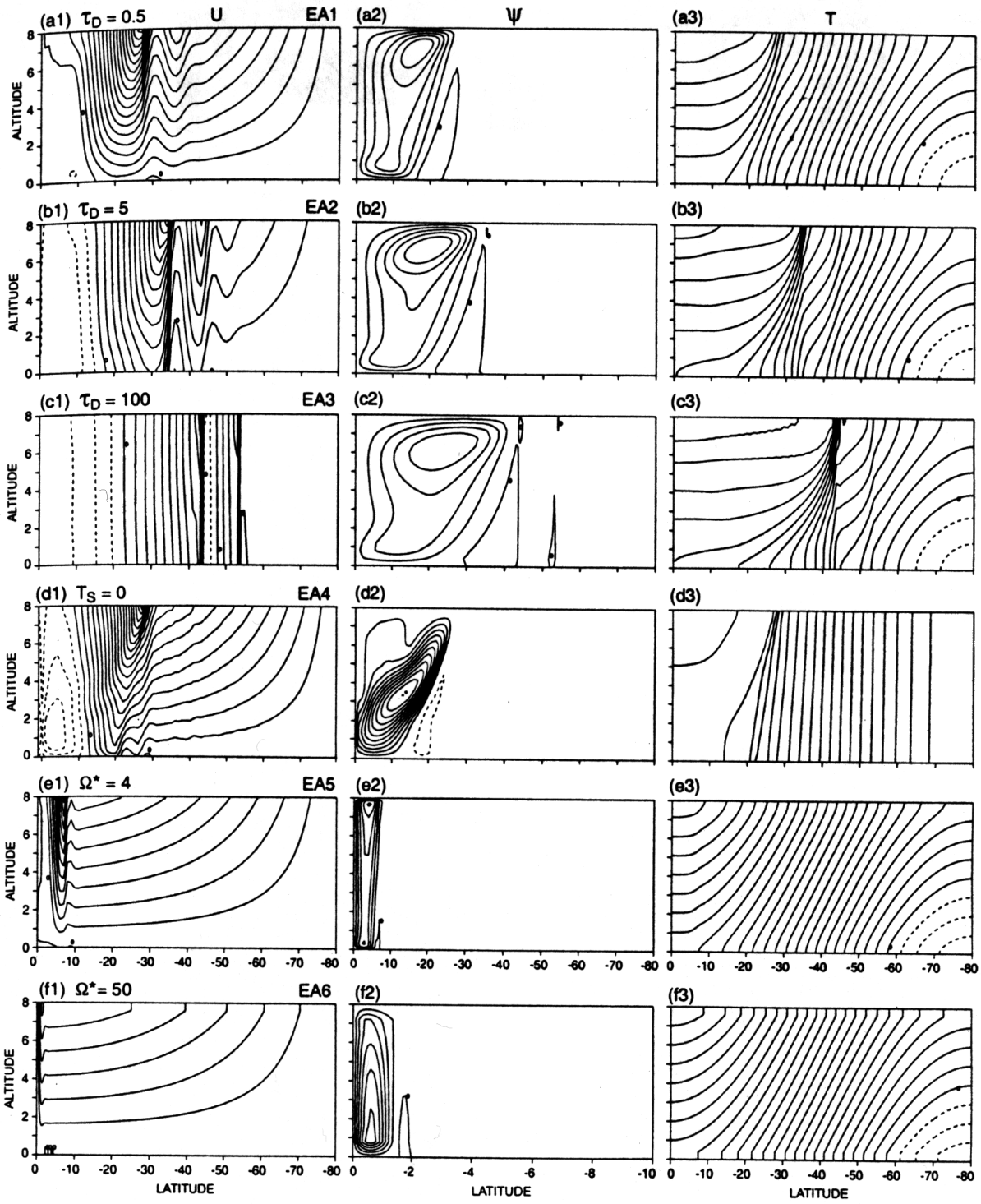

Fig. A1. Meridional sections of the zonal velocity, streamfunction, and temperature for the six terrestrial axisymmetric cases, EA1–EA6. The contour intervals are (a1) 5 m s^{-1}, (a2) 100 m^2 s^{-1}, (b1) 10 m s^{-1}, (b2) 500 m^2 s^{-1}, (c1) 20 m s^{-1}, (c2) 1000 m^2 s^{-1}, (d1) 5 m s^{-1}, (d2) 1000 m^2 s^{-1}, (e1) 2 m s^{-1}, (e2) 3 m^2 s^{-1}, (f1) 0.2 m s^{-1}, (f2) 1 m^2 s^{-1}. The temperature contour interval is 5°C, except for (c3) where it equals 2°C. The zero-value contour is omitted from the EA4 streamfunction plot.

Table A1. The basic parameters for the axisymmetric terrestrial cases in Figs. A1–A3. The cases examine the dependence on the drag rate, rotation rate, and static stability. All cases have a $P_2(\phi)$ heating profile, a structure with $S_1 = 1$ and $S_2 = z'$, and a heating rate of $\tau = 20$ days. The heating amplitudes, ΔT and δT, have °C units. The ν_4 and ν_2 diffusion coefficients have units of 10^{15} m^4 s^{-1} and 1 m^2 s^{-1}, respectively. The horizontal grid has $\Delta\phi = 1°$, except when $\Delta\phi = 0.1°$ for EA6. The vertical grid is uniform with $\Delta z = H/KZ$. The *time* column gives the extent of each calculation in units of 10^3 days.

Case	ΔT	δT	Ω^*	τ_D	ν_2	ν_4	KZ	time
EA1	100	40	1	0.5	1	0	50	1
EA2	100	40	1	5	1	0	50	4
EA3	35	15	1	100	1	0	20	50
EA4	100	0	1	0.5	1	0	50	2
EA5	100	40	4	0.5	0.1	0	50	10
EA6	100	40	50	0.5	0.01	0	10	2.5
EA7	50	20	1	∞	0	−1	10	30
EA8	25	10	1	∞	0	−0.3	10	400

in the zero-drag case, so no cell occurs. Thus the low-drag case, EA3, does not represent the zero-drag state, as we will see in section 3.5.

3.3 *Static stability limit*

For the classical theory to apply, the control state, EA1, requires the existence of a background static stability—provided by the δT term in (8)—even though it has no direct influence on the width of the Hadley cell. When this factor is omitted altogether, as in the EA4 solution in Fig. A1d, the Hadley cell becomes ten times stronger than in the control case, but still retains the canonical width. Both the upflow and downflow have a strong slope that allows the cell to produce its own static stability in low latitudes. In midlatitudes, small cells exist that also create a weak static stability and are generally noisy, which is why this one case is plotted using a time average. These cells seem to behave like the cells in the adiabatic regions of the Satoh's (1994) moist model, but whether they also migrate equatorward as his do was not determined. Nonetheless, the zonal flow still consists of two balanced components, though their meshing is different, with only one peak occurring, along with significant easterlies near the equator.

The EA4 solution suggests that aspects of the standard theory still hold even though certain underlying constraints are violated. Specifically, for a given dynamical or over-turning timescale, $\tau_d = (\tau\delta T)/(R\Delta T)$, the theory (Held and Hou 1980) requires that $\tau_d \gg \tau$ for consistency; otherwise the circulation will modify the static stability. The theory also requires that $\tau_d \gg 1/(\Omega R^{1/2})$ for the thermal wind balance in (18) to hold; otherwise the term $\nabla \cdot (\mathbf{v}v)$ will not be negligible compared to fu at $z = H$. It is surprising that the theory still applies at all, given that neither condition is met when $\delta T = 0$ in the EA4 case. The equality $\tau_d = \tau$ marks the transition to nonlinear balances in which the temperature is determined in a more complex way. Although the Hadley cell has the standard width, the processes controlling its amplitude are not understood.

3.4 *Rotation limit*

The cells do become narrower, however, when the rotation rate increases and this raises questions about what happens when $\Omega^* \to \infty$: do the same balances occur or is there some limit at which the dynamics changes? In examining these issues, the EA5 case in Fig. A1e shows that when $\Omega^* = 4$ the flow character already has some differences from the control case. For example, the cell slope is much re-

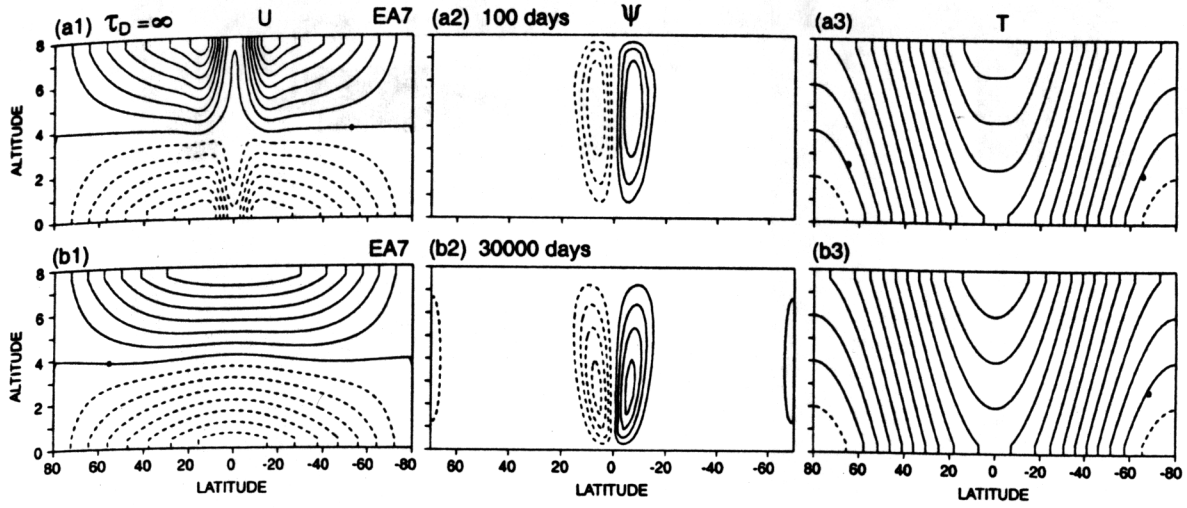

Fig. A2. Meridional sections of the zonal velocity, streamfunction, and temperature for the terrestrial, axisymmetric, zero-drag case, EA7 at 100 and 30000 days. In order, the contour interval, maximum and minimum values are (a1) $(2, 15, -14)$ m s^{-1}; (a2) $(20, 78, -78)$ m^2 s^{-1}; (a3) $(5, 58, -9)$°C; (b1) $(2, 14, -15)$ m s^{-1}; (b2) $(20, 87, -87) \times 10^{-4}$ m^2 s^{-1}; (b3) $(5, 59, -9)$°C. The zero-value contour is omitted from the streamfunction plots.

duced, even though the 6° cell width agrees with the theoretical value given by (22), and the value of the vertical viscosity is low enough to give a sloping cell should it exist. Because the cell is confined to such low latitudes, the usual thermal front is absent and the radiative temperature distribution prevails almost everywhere. Also absent is a secondary peak in the zonal flow, though the usual components still form an intense jet in low latitudes.

At even higher rotation rates, calculations with $\Omega^* = (10, 20, 50)$ produce Hadley cells with widths, $(3.2, 2.8, 1.5)°$, that differ significantly from the theoretical values, $(3, 1.5, 0.5)°$ when Ω^* is greater than 15. According to the EA6 case with $\Omega^* = 50$ in Fig. A1f, the cells and jet disappear gradually as the rotation rate approaches the upper limit, but with some deviation from the theory. An extra-high resolution and a low viscosity in this case guarantee that the features, particularly the broad poleward flow aloft, are not numerically dependent. Thus at high rotation rates, the cell really is two to three times wider than expected from the theory and its poleward flow really is no longer confined to the upper boundary. A thermal wind exists to within a degree of the equator where the usual jet still forms, though it only reaches 1.2 m s^{-1} in amplitude.

The theoretical constraints that are violated in the EA6 case are those that require the poleward flow to be confined to the upper boundary and those that assume that the advection term $\nabla \cdot (\mathbf{v}v)$ is negligible compared to fu at $z = H$ in (18). These conditions are less likely to hold in a narrow cell that remains so confined to the equatorial zone. Otherwise, the theory holds up remarkably well as the $\Omega^* \to \infty$ limit is approached.

3.5 *Zero-drag limit*

Although flows with a zero drag and zero vertical viscosity form a special group, steady solutions to the equations can still be found provided that a weak horizontal viscosity is activated to control the numerics in a global domain.[6] Thus, when the viscosity coefficient exceeds a critical value, $\nu_4^c \approx -5 \times 10^{14}$ m^4 s^{-1}, steady flows such as EA7 in Fig. A2 can be produced. Most terms in the prediction equations are close to zero, but the weak supercritical diffusion allows the thermal wind

$$u = \left(\frac{\alpha g H \Delta T}{2\Omega}\right)(z' - 0.5)\cos\phi, \tag{24}$$

6 Two hemispheres are chosen to avoid activating any small numerical terms near the equator.

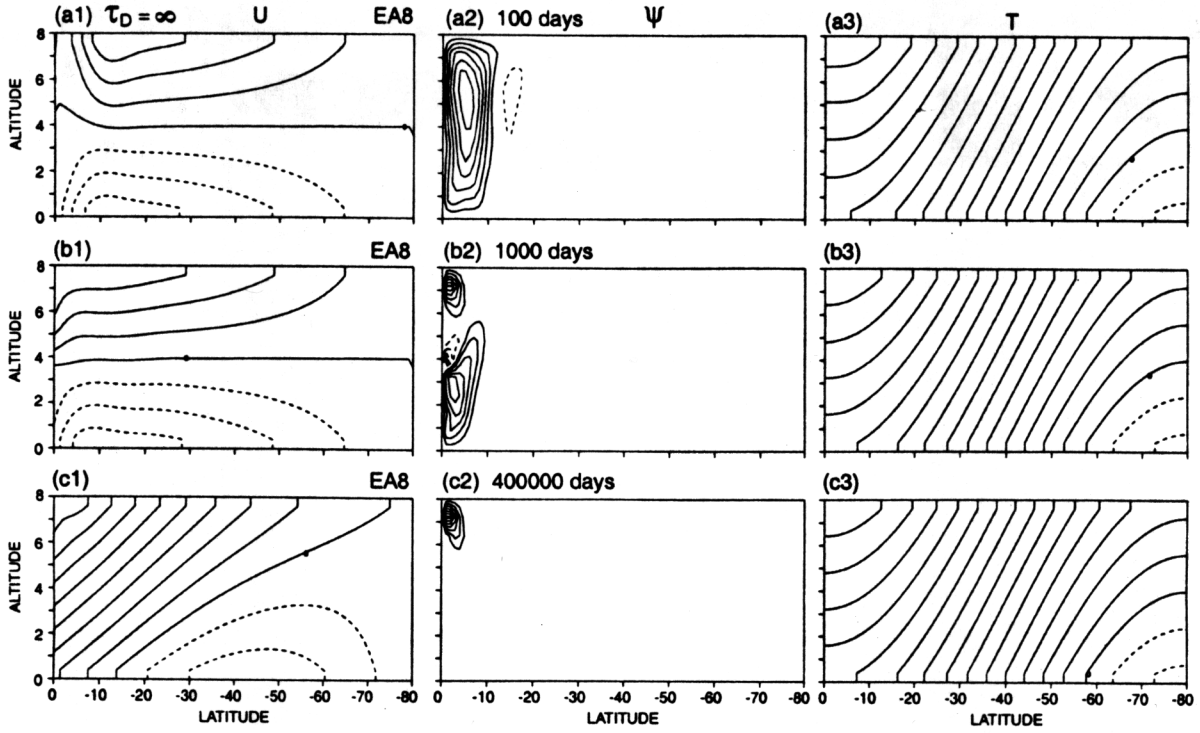

Fig. A3. Meridional sections of the zonal velocity, streamfunction, and temperature for the terrestrial, axisymmetric, zero-drag case, EA8 at 100, 1000, and 400000 days. In order, the contour interval, maximum and minimum values are (a1) $(2, 7.6, -7.0)$ m s^{-1}; (a2) $(5, 33, -6)$ m^2 s^{-1}; (b1) $(2, 7.4, -7.0)$ m s^{-1}; (b2) $(1, 6.1, -4.4)$ m^2 s^{-1}; (c1) $(2, 16.8, -5.2)$ m s^{-1}; (c2) $(1, 7.6, -0.6)$ m^2 s^{-1}; together with $(2, 29, -4)$°C for all the temperature fields. The zero-value contour is omitted from the streamfunction plots.

to emerge at all latitudes. The weak terms also produce weak Hadley cells.

Initially, the EA7 zonal flow is zero at the equator but it soon changes as the thermal wind spreads from middle to low latitudes, Fig. A2a. A quasi-steady thermal wind forms in about 3000 days, but the spindown of the meridional cells takes much longer. The cells at the equator are weak initially, and become much weaker by a factor of 10^4 in Fig. A2b, though their form remains unchanged. The final westerly and easterly components are equal as the initial momentum is zero.

A thermal wind also emerges in the second example, EA8 in Fig. A3, but does not reach a steady state due to small differences in the mixing when the domain is hemispheric. The zonal flow can be represented by the empirical form

$$u = U_0 \cos\phi[z' - 0.5 - a_1(t)\sin\phi + a_2(t)], \tag{25}$$

where $U_0 = 15.5$ m s^{-1} is constant, but the other factors vary such that $a_1 = (0, 0.7, 1.08)$ and $a_2 = (0, 0.5, 0.7)$ when $t = (1, 100, 400) \times 10^3$ days. Such a flow is equivalent to a steady thermal wind plus a slow growing barotropic component whose source may be physical, but could be numerical given that the finite difference equations do not conserve all quadratic quantities. The associated cells are gradually reduced to a small recirculation aloft near the equator. Although this system does not equilibrate, the rate of change is extremely slow.

Together, the zero-drag solutions show that a global thermal wind is possible but that its occurrence is highly dependent on a numerical formulation that prevents the equations from becoming slowly divergent.

3.6 Rotation range

For reference and completeness, consider next how the axisymmetric circulation varies over a full range of rotation rates, using the jo-

Table B1. The basic parameters for the thick axisymmetric jovian cases as a function of rotation rate in Fig. B1. All cases have heating amplitudes of $\Delta T = \delta T = 0.1°C$, a $P_2(\phi)$ heating profile, a structure with $S_1 = 1$ and $S_2 = z'$, a heating rate of $\tau = 300$ days, and a drag rate of $\tau_D = 30$ days. The ν_2 coefficient has units of 10^4 m^2 s^{-1}, while $\nu_4 = 0$. The horizontal grid has $\Delta\phi = 1°$, except when $\Delta\phi = 0.5°$ for JA1. The vertical grid is uniform with $KZ = 20$. The *time* column gives the extent of each calculation in units of 10^3 days.

Case	Ω^*	ν_2	time
JA1	1	0.5	100
JA2	1/2	1	200
JA3	1/4	2	150
JA4	1/8	10	30
JA5	1/16	20	20
JA6	1/32	50	10
JA7	1/64	50	10

vian parameters for variety in the cases JA1–JA7 of Fig. B1 and Table B1. Each jovian circulation is equivalent to a terrestrial flow at a higher rotation rate. As noted in section 2.2, some jovian parameters are arbitrary so the nominal depth can be decreased and the temperature increased proportionally in the solutions to give similar flows. The basic parameters are chosen to give a zonal velocity of about 20 m s^{-1}, as well as an easily resolved cell, at $\Omega^* = 1$.

The circulations in Fig. B1 progress in agreement with the theory of Held and Hou (1980), particularly over the medium range defined by $\Omega^* = 1/16$ to 1/4, with the Hadley cell becoming narrower as the rotation rate increases, almost halving from frame to frame. However, some deviations from the theory are apparent in the high and low rotation ranges. For example, in the high range defined by $\Omega^* = 1/2$ to 1, the zonal wind balance no longer produces a second jet peak, the temperature field no longer deviates much from the radiative form, and the Hadley cell no longer slopes.

In the low range, defined by $\Omega^* = 1/32$ to 1/64, the flows have extensive easterlies in low latitudes and the secondary jet is again absent, probably because the U_R wind is so narrow and the U_A wind is so broad. The temperature field is correspondingly uniform in low latitudes, with the front at the cell boundary becoming sharper as the cell extends farther poleward. The secondary cells that form near the surface just outside the Hadley cell have the characteristics of axisymmetric instabilities. In the limit of no rotation (not shown), the Hadley cell reaches the pole and becomes more symmetrical in the vertical, whereas at other rotation rates it tends to be stronger aloft.

3.7 *Vertical transitions*

Other transitions occur in the jovian system when the LIN heating confines the flow to thin layers. In examining these effects, most of the calculations use a slower rotation rate, $\Omega^* = 1/4$, so as to develop a wider, more-easily resolved Hadley cell for the JB subset in Fig. B2 and Table B2. The first three cases show how the circulation changes as the depth of the heated layer goes from thick to thin, with $h = (H, H/4, H/30)$. These calculations activate a ν_4 diffusion so as to accelerate the convergence of the solution, which tends to be slow when the cells are narrow. This results in a shorter integration time for the thick reference case, JB1, which otherwise resembles the basic JA3 case. In the two thinner sytems, JB2 and JB3, the zonal flow is confined aloft, though still made up of the usual U_A and U_R components. Their Hadley cells still reach the bottom surface but are vertically bimodal, with the component in the heated layer being stronger and slightly wider than the component in the unheated sublayer. The cell widths are the same as those given by the basic theory, provided that the scale h, not H, is used to define the R parameter in (23).

The circulations described by the classical theory also depend to some extent on the form chosen for the latitudinal heating profile, $P(\phi)$ in (8), especially near the equator. To examine this factor in the JB4 case, the usual P_2 distribution is replaced by the P_{BT+BC} form in which the heating profile is uniform (barotropic) from the equator to 15° and then linear (baroclinic) in latitude thereafter. For a thin layer with $h = H/2$, this profile produces a jet and cell that are centered at the edge of the baroclinic zone at 15°, rather than at the equator, Fig. B2d. Such a displacement occurs when the baro-

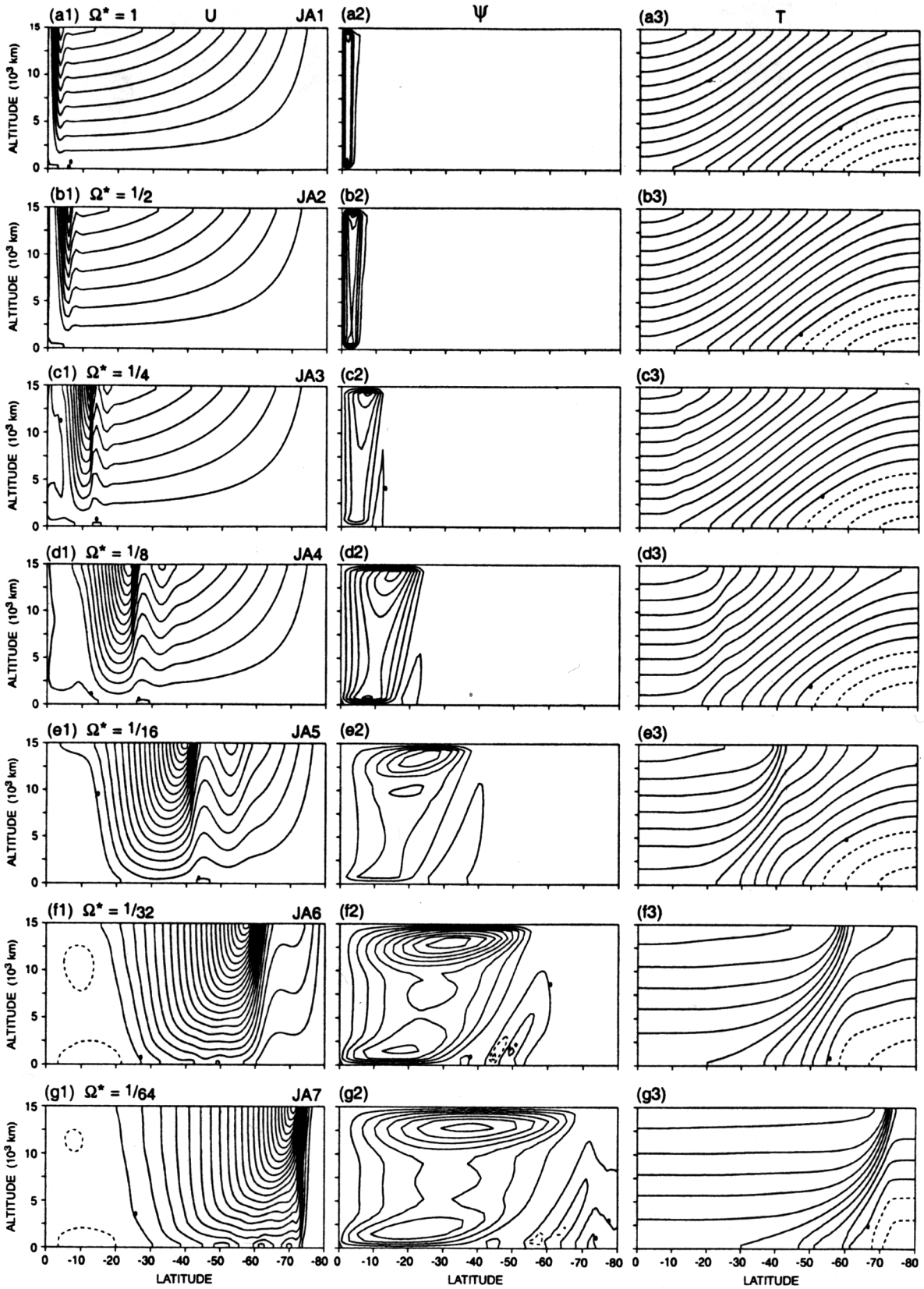
(a1) Ω* = 1
U
JA1
(a2)
Ψ
(a3)
T
(b1) Ω* = 1/2
JA2
(b2)
(b3)
(c1) Ω* = 1/4
JA3
(c2)
(c3)
(d1) Ω* = 1/8
JA4
(d2)
(d3)
(e1) Ω* = 1/16
JA5
(e2)
(e3)
(f1) Ω* = 1/32
JA6
(f2)
(f3)
(g1) Ω* = 1/64
JA7
(g2)
(g3)
ALTITUDE (10³ km)
0
5
10
15
0 -10 -20 -30 -40 -50 -60 -70 -80
LATITUDE

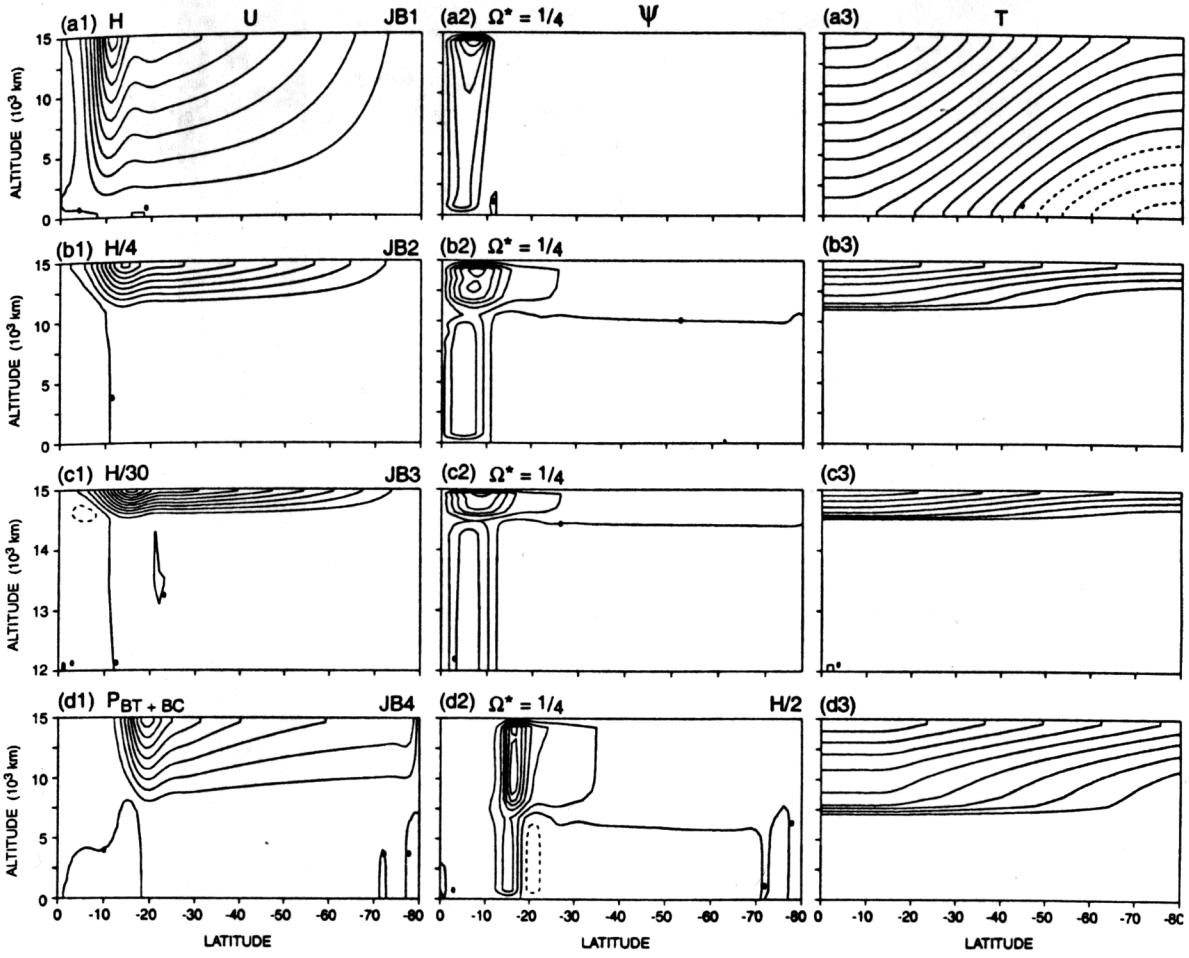

Fig. B2. Meridional sections of the zonal velocity, streamfunction, and temperature for the jovian axisymmetric cases with different thicknesses (JB1–JB3) and a different heating profile (JB4). In order, the contour interval, maximum and minimum values are (a1) $(10, 95, -1)$ m s^{-1}; (a2) $(10, 58, -0) \times 10^3$ m^2 s^{-1}; (a3) $(1, 14, -4) \times 10^{-2}$°C; (b1) $(10, 82, -8)$ m s^{-1}; (b2) $(2, 11, -2) \times 10^3$ m^2 s^{-1}; (b3) $(1, 7.6, 0) \times 10^{-1}$°C; (c1) $(10, 104, -15)$ m s^{-1}; (c2) $(4, 21, -3) \times 10^2$ m^2 s^{-1}; (c3) $(1, 7.6, -0)$°C; (d1) $(10, 85, -2)$ m s^{-1}; (d2) $(10, 68, -14) \times 10^2$ m^2 s^{-1}; (d3) $(4, 39, 0) \times 10^{-2}$°C.

tropic zone is wider than the cell itself. Apparently, the equator is less important in determining the circulation than is the latitude at which the baroclinicity begins.

4. Terrestrial states

The theory for the 3-D terrestrial circulation is well developed, and primarily involves explaining the functioning of the underlying nonlinear baroclinic instability—see the review by Held and Hoskins (1985). This section is concerned with testing the theoretical limits by examining how the unstable mode depends on the imposed heating distribution, the static stability, and the surface drag. An alternative state, with two jets per hemisphere, is also dis-

Fig. B1. Meridional sections of the zonal velocity, streamfunction, and temperature showing the rotational range of the jovian axisymmetric cases JA1–JA7. The contour intervals are (a1) 2 m s^{-1}, (a2) 2×10^2 m^2 s^{-1}, (b1) 5 m s^{-1}, (b2) 1×10^3 m^2 s^{-1}, (c1) 10 m s^{-1}, (c2) 1×10^4 m^2 s^{-1}, (d1) 15 m s^{-1}, (d2) 5×10^5 m^2 s^{-1}, (e1) 20 m s^{-1}, (e2) 5×10^5 m^2 s^{-1}, (f1) 20 m s^{-1}, (f2) 10×10^5 m^2 s^{-1}, (g1) 20 m s^{-1}, (g2) 2×10^6 m^2 s^{-1}. The temperature contour interval is 1×10^{-2}°C.

Table B2. The basic parameters for the axisymmetric jovian cases in Fig. B2. The cases primarily show the dependence on the relative thickness, h'. The heating profile P_{BT+BC} is barotropic with a value of unity from the equator to $\phi = 15°$, then baroclinic until vanishing at 80°. The thick structure has $S_1 = 1$ and $S_2 = z'$, while the thin has $S_1 = C[1, 0]$ and $S_2 = C[z_c^2, 0]$. The heating rate has $\tau = 300$ days, while the drag has $\tau_D = 30$ days. The heating amplitudes, ΔT and δT, have °C units. The ν_4 and ν_2 coefficients have units of 10^{16} m^4 s^{-1} and 10^4 m^2 s^{-1}, respectively. The horizontal grid has $\Delta\phi = 1°$. The vertical grid is uniform for most cases but split for JB3. The vertical resolution has $KZ = 20$. The *time* column gives the extent of each calculation in units of 10^3 days.

Case	h'	Ω^*	ΔT	δT	$P(\phi)$	$S(z)$	ν_2	ν_4	time
JB1	1	1/4	0.1	0.1	P_2	thick	2	−1	50
JB2	1/4	1/4	0.4	0.4	P_2	thin	0.5	−1	50
JB3	1/30	1/4	4	4	P_2	thin	0.01	−1	60
JB4	1/2	1/4	0.2	0.2	P_{BT+BC}	thin	1	−1	60

cussed. The resulting E1–E6 set of solutions also gives some measure of how much the storm tracks, and jet locations can vary for even the simplest system.

4.1 *Basic states*

The first two cases, E1 and E2 in Figs. C1 and C2 and Table C1, define the range of states that can exhibit regular jets under the basic heating arrangement. The E1 solution with $\Delta T = 30$°C represents flow at the low heating limit, while the E2 case with $\Delta T = 60$°C describes the high heating limit. At lower rates, the flows tend be baroclinically stable, while at higher rates, such as $\Delta T = 70$°C, regular behavior ends and the jet oscillates wildly. These, and other solutions, show that the mean jet axis lies at $\phi = (34, 43, 46, 50, 50)°$ when $\Delta T = (30, 40, 50, 60, 70)$°C, respectively.[7] The jet location appears to depend as much on the heating amplitude as on the heating profile, $P_2(\phi)$. Furthermore, the locations do not vary continuously but, rather, appear to be quantized by the dominant eddy scale, jumping from near 35° to the 45°–50° zone as ΔT is increased.

The E1 control circulation in Fig. C1 represents an idealized version of the annual mean terrestrial state: the jet at 34° is bounded by surface easterlies in low and high latitudes,

7 With δT fixed at 40°C for these cases.

Table C1. The basic parameters for the terrestrial cases in Figs. C1–C6. The heating profile equals $P_2(\phi)$ except when it equals P_{DIP} for E6, where $g(15°, 10°, -0.5)$ defines the center, half-width, and amplitude of the Gaussian cooling dip imposed upon a P_{BT+BC} component. The P_{BT+BC} heating is barotropic with a value of unity from the equator to $\phi = 15°$, then baroclinic until vanishing at 70°. All cases have a thick structure with $S_1 = 1$ and $S_2 = z'$. The heating rate has $\tau = 20$ days. The heating amplitudes, ΔT and δT, have °C units. The diffusion coefficients are $\nu_4 = -10^{15}$ m^4 s^{-1} and $\nu_2 = 0.5$ m^2 s^{-1}, except for E5 when $\nu_4 = -0.2 \times 10^{15}$ m^4 s^{-1} and $\nu_2 = 0$. The vertical grid is uniform with $KZ = 20$. The horizontal grids have $\Delta\phi = 1°$ and $\Delta\lambda = 3°$ over a 180° domain, except for E5 when $\Delta\lambda = 1°$ over a 60° domain. The *time* column gives the extent of each calculation in units of 10^3 days, while τ_D is in days.

Case	ΔT	δT	Ω^*	τ_D	time
E1	30	40	1	1	1
E2	60	40	1	1	1
E3	30	0	1	1	1
E4	30	40	1	50	1.5
E5	70	40	4	1	1
E6	40	40	1	1	1

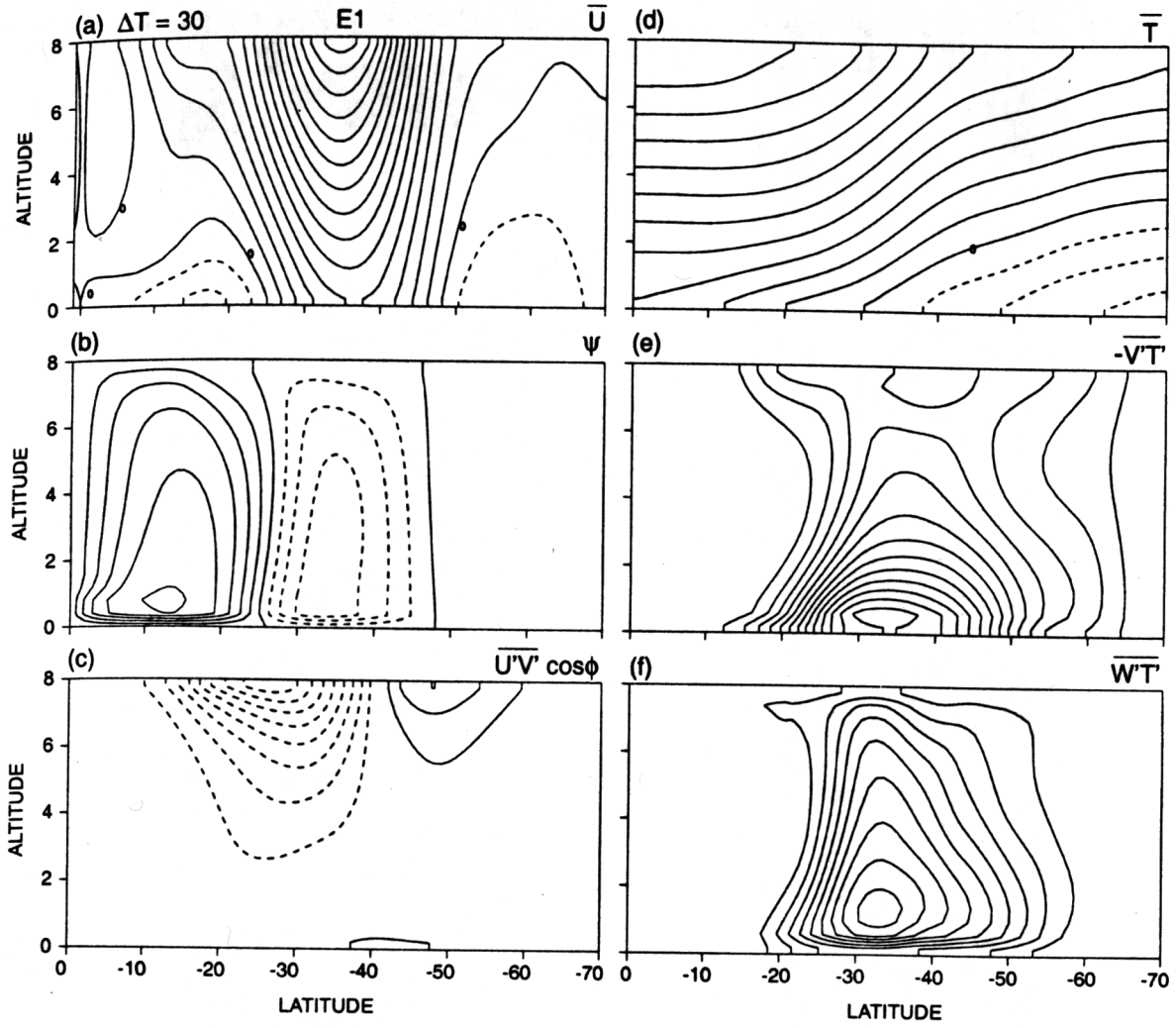

Fig. C1. Meridional sections of the primary fields and eddy transports for the basic terrestrial E1 case with a low baroclinicity (ΔT). The means are based on daily averages taken over 900–1000 days. In order, the contour interval, maximum and minimum values are (a) $(2, 29, -4)$ m s^{-1}; (b) $(1, 5.2, -3.5) \times 10^2$ m^2 s^{-1}; (c) $(2, 6.0, -17.4)$ m^2 s^{-2}; (d) $(4, 44, -13)$°C; (e) $(0.5, 6.8, -0.1)$°C m s^{-1}; (f) $(0.5, 4.7, -0.1) \times 10^{-3}$°C m s^{-1}. The zero-value contours are omitted for the eddy fields.

and is accompanied by a weak thermal front and by Hadley and Ferrel cells with 25° widths. On the other hand, in the high baroclinicity E2 case in Fig. C2, the two cells are twice as strong and occupy the whole hemisphere, while the jet at 50° has surface easterlies only on the equatorward side. As regards the eddies, their kinetic energy (not shown) peaks in the jet cores, with latitudinal distributions that are symmetric in the E1 case, but asymmetric in the E2 case. The enstrophy zonal spectra also differ, with the orderly E1 flow having a sharp peak at wavenumber eight and the irregular E2 flow not having any really dominant mode.

The baroclinic instabilities, as defined by the eddy heat fluxes, also differ, being centered near the ground at the jet axis in the E1 case but equatorward of the axis, at 40°, in the E2 case. Both the poleward and upward heat fluxes, $-\overline{v'T'}$ and $\overline{w'T'}$, are strongest near the ground (in keeping with linear instability theory) in the E1 case, but are also strong aloft in the E2 flow. In both cases, the eddy momentum flux, $\overline{u'v'}$, is produced by planetary waves

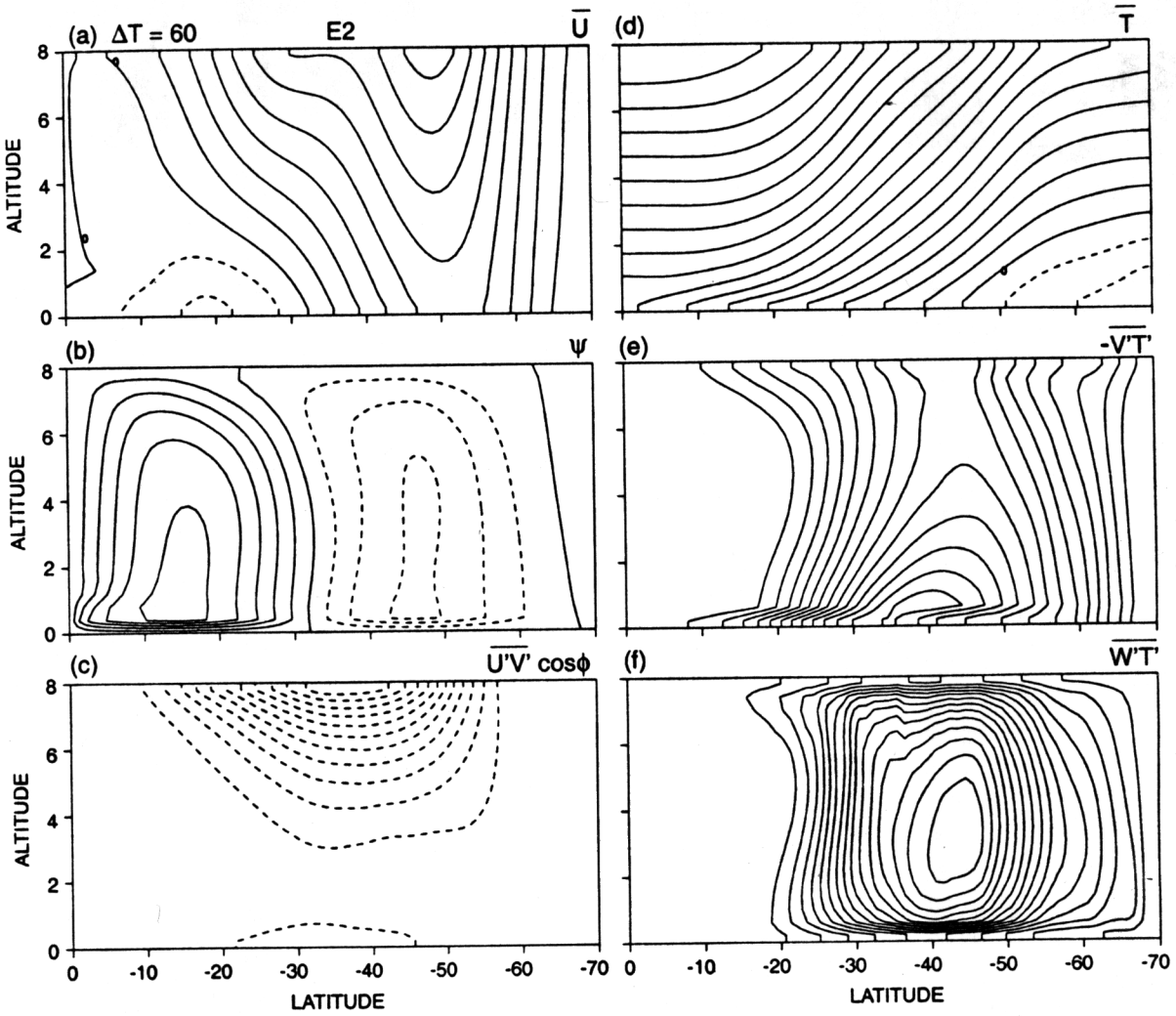

Fig. C2. Meridional sections of the primary fields and eddy transports for the basic terrestrial E2 case with a high baroclinicity (ΔT). The means are based on daily averages taken over 800–1000 days. In order, the contour interval, maximum and minimum values are (a) $(5, 43, -11)$ m s^{-1}; (b) $(2, 10.7, -6.4) \times 10^2$ m^2 s^{-1}; (c) $(5, 2.5, -59.4)$ m^2 s^{-2}; (d) $(4, 72, -11)$°C; (e) $(1, 13.8, -0.5)$°C m s^{-1}; (f) $(1, 15.7, -0.3) \times 10^{-3}$°C m s^{-1}. The zero-value contours are omitted for the eddy fields.

that are generated aloft after the instability has transferred the energy upward. These waves only propagate equatorward in the E2 case, according to a $\overline{u'v'}$ flux that is entirely poleward traversing, but also propagate poleward in the E1 case, according to the converging flux. The vertical eddy momentum flux (not shown) correlates closely with the meridional flux in both cases, in keeping with the relationship $B\overline{u'w'} \sim T_\phi \overline{u'v'}$ of linear theory; this suggests that the eddy dynamics are primarily quasi-geostrophic.

These differences between the basic low and high baroclinicity states suggest that the nature of the nonlinear baroclinic instabilities depends on the scale of the eddies, and the latitude at which they are generated. Existing theory could be extended to allow for these factors.

4.2 *Zero static stability*

The next case, E3 in Fig. C3, examines what happens to the circulation when the background static stability is omitted. This factor

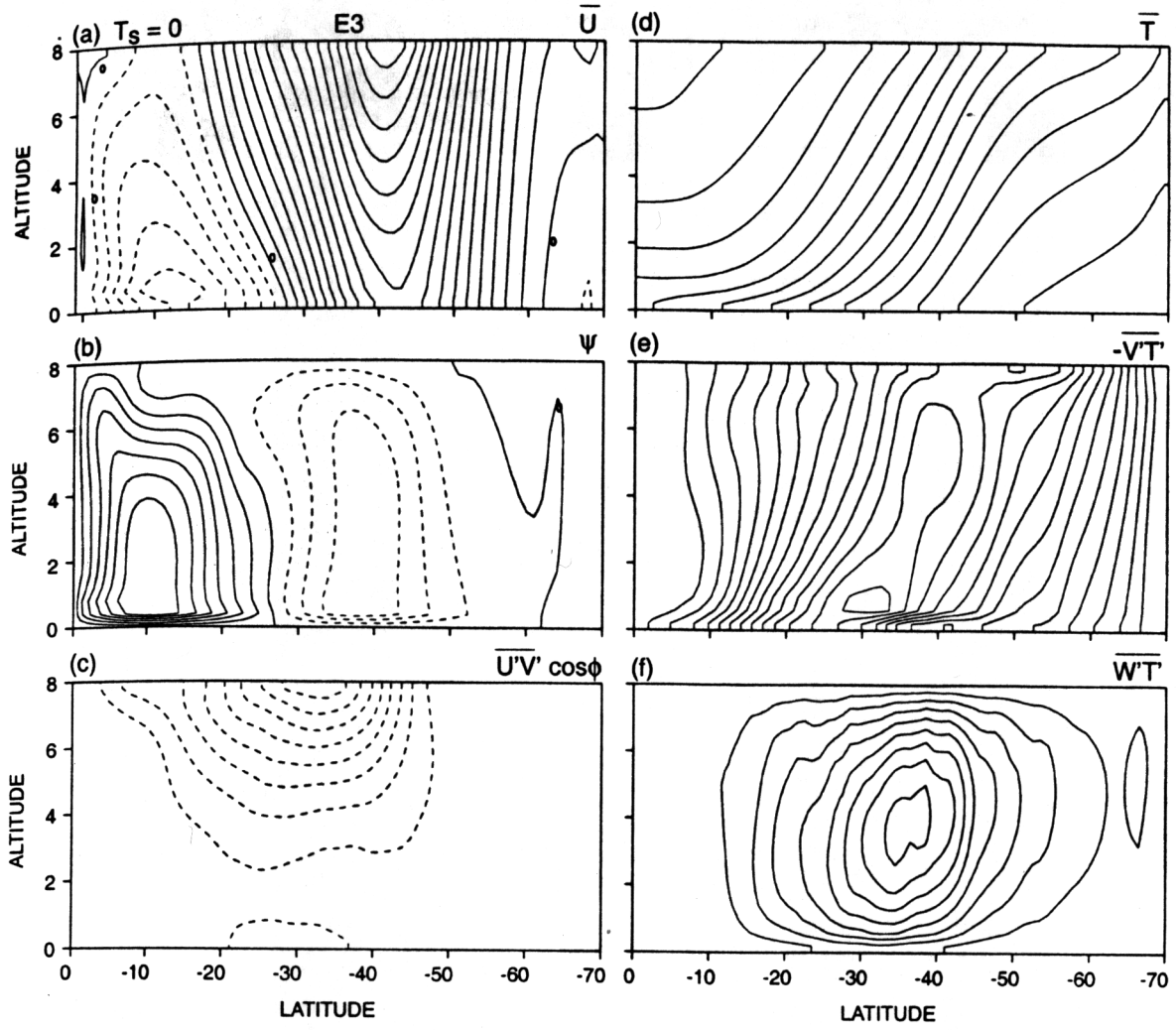

Fig. C3. Meridional sections of the primary fields and eddy transports for the terrestrial E3 case with no background static stability. The means are based on daily averages taken over 800–1000 days. In order, the contour interval, maximum and minimum values are (a) $(2, 32, -11)$ m s^{-1}; (b) $(2, 14.0, -7.2) \times 10^2$ m^2 s^{-1}; (c) $(5, 3.2, -43.1)$ m^2 s^{-2}; (d) $(2, 29, 2)$°C; (e) $(0.5, 6.7, -0.1)$°C m s^{-1}; (f) $(2, 16.8, -1.5) \times 10^{-3}$°C m s^{-1}. The zero-value contours are omitted for the eddy fields.

is crucial to the baroclinic instability process according to linear quasi-geostrophic theory. However, in the nonlinear system the instability still occurs and stabilizes the flow in mid-latitudes by advecting heat upward. The Hadley cell does the same in low latitudes, just as it did in the axisymmetric EA4 case, by becoming much stronger while keeping its width at the control value. Stronger easterlies now occupy low latitudes, again as in the EA4 case.

Of the eddy fluxes, $\overline{u'v'}$ and $\overline{w'T'}$ are about three times stronger than their E1 counterparts, while $\overline{v'T'}$ is about the same although it is now equally strong at all heights. This flux also has a distinctive poleward slope, with the peak going from a latitude of 30° at the ground to 40° at the top. Although the $\overline{u'v'}$ flux traverses monotonically poleward across the jet, it does so only in the equatorward flank, despite the fact that the eddies are active throughout the hemisphere. Again, the $\overline{u'w'}$ flux (not shown) correlates well with $\overline{u'v'}$ flux so the dynamics may be close to being quasi-geostrophic for some aspects. Together, these features sug-

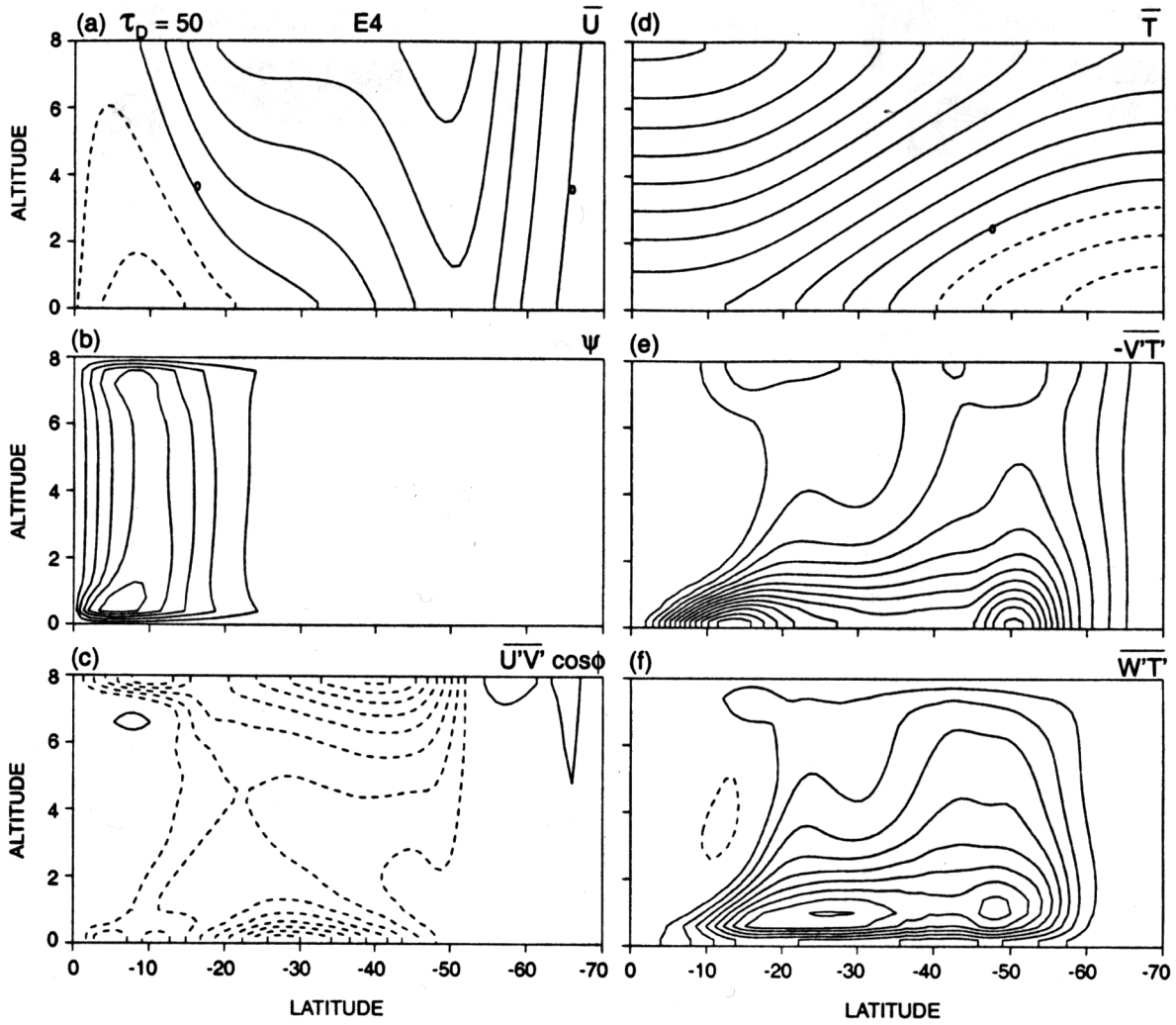

Fig. C4. Meridional sections of the primary fields and eddy transports for the terrestrial E4 case with a weak surface drag. The means are based on daily averages taken over 100–1500 days. In order, the contour interval, maximum and minimum values are (a) $(5, 23, -13)$ m s^{-1}; (b) $(2, 11.0, -0.7) \times 10^1$ m^2 s^{-1}; (c) $(1, 1.5, -8.4) \times 10^{-1}$ m^2 s^{-2}; (d) $(4, 45, -15)$°C; (e) $(0.5, 6.8, -0.2) \times 10^{-1}$°C m s^{-1}; (f) $(0.3, 2.7, -0.4) \times 10^{-4}$°C m s^{-1}. The zero-value contours are omitted for the eddy fields.

gest that the baroclinic instability is deeper and produces larger, more widespread eddies than in the control state.

The E3 solution, by having no set static stability, complements those basic states and theories that assume some arbitrary vertical distribution of temperature. To understand such an instability process, and how it generates its own static stability, perhaps the advective model developed by Fjortoft (1951) and Wiin-Nielsen (1967) for zero static stability—see section 2.4—can be extended to the nonlinear state to explain the eddy fluxes.

4.3 *Low drag*

When the drag is weakened by setting τ_D = 50 days, the character of the flow actually changes while the system slowly evolves towards equilibrium. Thus the E4 state in Fig. C4 is defined using a mean taken over the whole integration period, rather than by a sample taken at the end. In some situations,

flows can be generated by baroclinic instabilities that are eventually suppressed by the mature flow, which then lacks clues as to how it originated. For such systems only a full-period average contains the full story. Paradoxically, some drag is needed to maintain the instability and the flow history.

Compared to the control case, the E4 mean jet lies in higher latitudes and has more of a barotropic component, but also has a weaker amplitude because the driving eddies are weaker. Similarly, the Hadley cell has only 1/5 the strength of the control cell, and the Ferrel cell barely exists. The cells are weak because, when the drag is weak, they exist more to compensate the eddy heat flux than to transfer momentum vertically. Recall, however, that in the low-drag axisymmetric case, EA3, the Hadley cell is actually stronger and wider than in the control state. This implies that the E4 cell is not an axisymmetric mode, but rather is a weak eddy-driven mode.

To be more specific, the eddy fluxes are an order of magnitude weaker than their control counterparts. According to the eddy heat fluxes, the baroclinic instability is relatively weak, shallow and has centers in low and high latitudes; these appear to be due to a single mode that peaks at the edges of the domain rather than being due to two lots of instability. Although weaker overall, the eddy momentum flux is equally active near the ground where it traverses poleward into the jet core. However, given the length of the averaging period and the changing flow character, it is possible that components of the eddy transports occur at different times in the different regions.

Solutions for systems with a weak surface drag have been discussed for a quasi-geostrophic model by Williams (1979), for a primitive equation model by James and Gray (1986) and James (1987), and for a GCM by Williams (1988). All models produce flows with weak eddy heat transports confined to low levels and all have baroclinic instabilities that are suppressed by the strong barotropic shears that develop. James' (1987) analysis explains how the lateral shear tries to suppress the instability by constraining the structure of the normal modes, confining them meridionally, and developing strong horizontal phase tilts that reduce the growth rates by returning the eddy energy to the barotropic component. Such strong lateral shears only exist when the drag is weak. Jets can also develop in such a way that they switch the baroclinic eddy source off completely (Williams 2003a). Clearly, a better understanding is needed of how eddy cascades can act to eliminate the source of the eddy activity.

4.4 *Double jets*

The character and location of the baroclinic instabilities can also be varied by developing them in double jet flows. This can be done either by increasing the rotation rate, or by introducing an additional source of baroclinicity (Williams 1988, 2003a,b). The two examples, cases E5 and E6 in Figs. C5 and C6, illustrate such variations in the nonlinear instability and, in passing, show how to produce jets in lower and higher latitudes.

First, in the E5 case, the rotation rate is quadrupled, with the baroclinicity doubled so as to attain the usual velocity range. This leads to smaller baroclinic eddies that drive two jets whose locations, 18° and 45°, differ significantly from their values, 35° and 65°, for a dry GCM (Williams 1988), due no doubt to differences in the heating schemes. In the meridional flow, the Ferrel cells coincide with the baroclinic instabilities and have about half the strength and half the width of the those in the E1 control case, in keeping with the smaller eddy scale.

Being smaller, the baroclinic eddies generate planetary waves that can propagate both poleward and equatorward. These produce eddy mometum fluxes, $\overline{u'v'}$, that converge on the low latitude jet and traverse poleward across the midlatitude jet. How the two wave sets interact is unknown, but the eddy kinetic energy field (not shown) peaks within the jets and has only a weak contribution elsewhere, suggesting that the jets are almost self contained as regards the momentum. However, the lateral heat flux, $\overline{v'T'}$, remains continuous between the two jets. In an unusual distribution, the vertical heat flux, $\overline{w'T'}$, has one peak near the ground and one at mid-height, a measure of how the two instabilities can coexist and vary with location.

The second case, E6 in Fig. C6, shows that double jets can also be generated by adding a low-latitude source of baroclinicity to a standard midlatitude source. This is done by adding

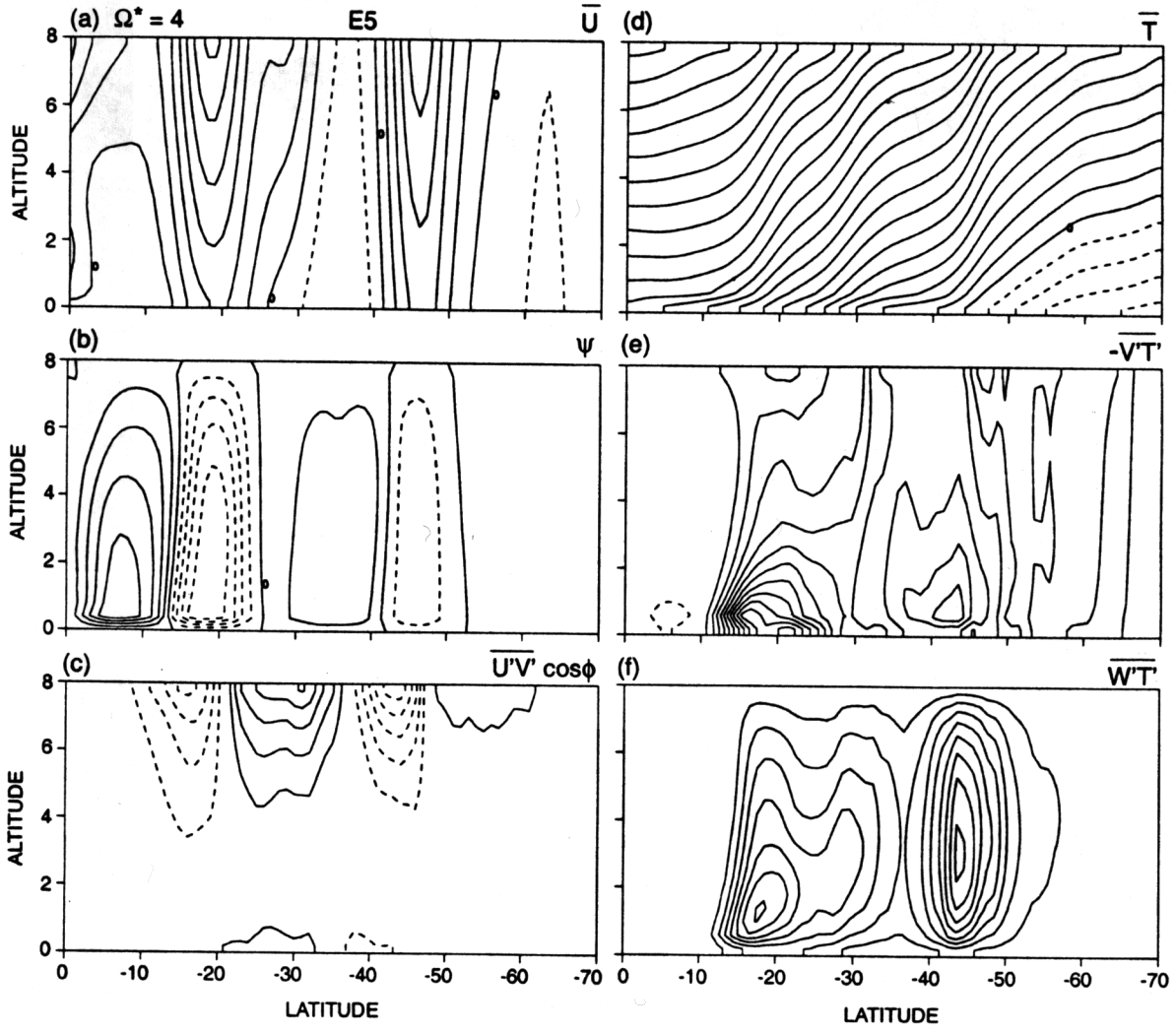

Fig. C5. Meridional sections of the primary fields and eddy transports for the terrestrial E5 case with double jets produced by a high rotation rate. The means are based on daily averages taken over 950–1000 days. In order, the contour interval, maximum and minimum values are (a) $(5, 31, -9)$ m s^{-1}; (b) $(0.5, 2.4, -2.3) \times 10^2$ m^2 s^{-1}; (c) $(2, 10.2, -11.2)$ m^2 s^{-2}; (d) $(4, 89, -17)$°C; (e) $(0.5, 5.7, -1.0)$°C m s^{-1}; (f) $(1, 8.2, -0.2) \times 10^{-3}$°C m s^{-1}. The zero-value contours are omitted for the eddy fields.

a Gaussian cooling dip at 15° to a simple P_{BT+BC} heating distribution, thereby producing the P_{DIP} profile—see Fig. 2.[8] This results in a near-axisymmetric jet in low latitudes that coexists with the eddy-driven jet, which now lies in higher latitudes. Although the main Hadley cell is axisymmetric, the neighboring Ferrel cell is eddy driven; both cells are twice as strong as in the control case. The eddies are mainly confined to high latitudes where they are large and produce fluxes of heat and momentum similar to the control case. However, in low latitudes, a stronger equatorial superrotation could also be added to the circulation by making the low-latitude jet stronger and sufficiently barotropically unstable to produce the necessary eddy driving—see Williams (2003b) for a detailed discussion.

8 A more systematic approach would involve setting $P(\phi) = c_2 \cdot \cos^2\phi + c_n \cdot \cos^n\phi$, where c_2 and c_n are constants ≤ 1 for $n = 4$, 8, 16 or 32, as in Williams (2003b).

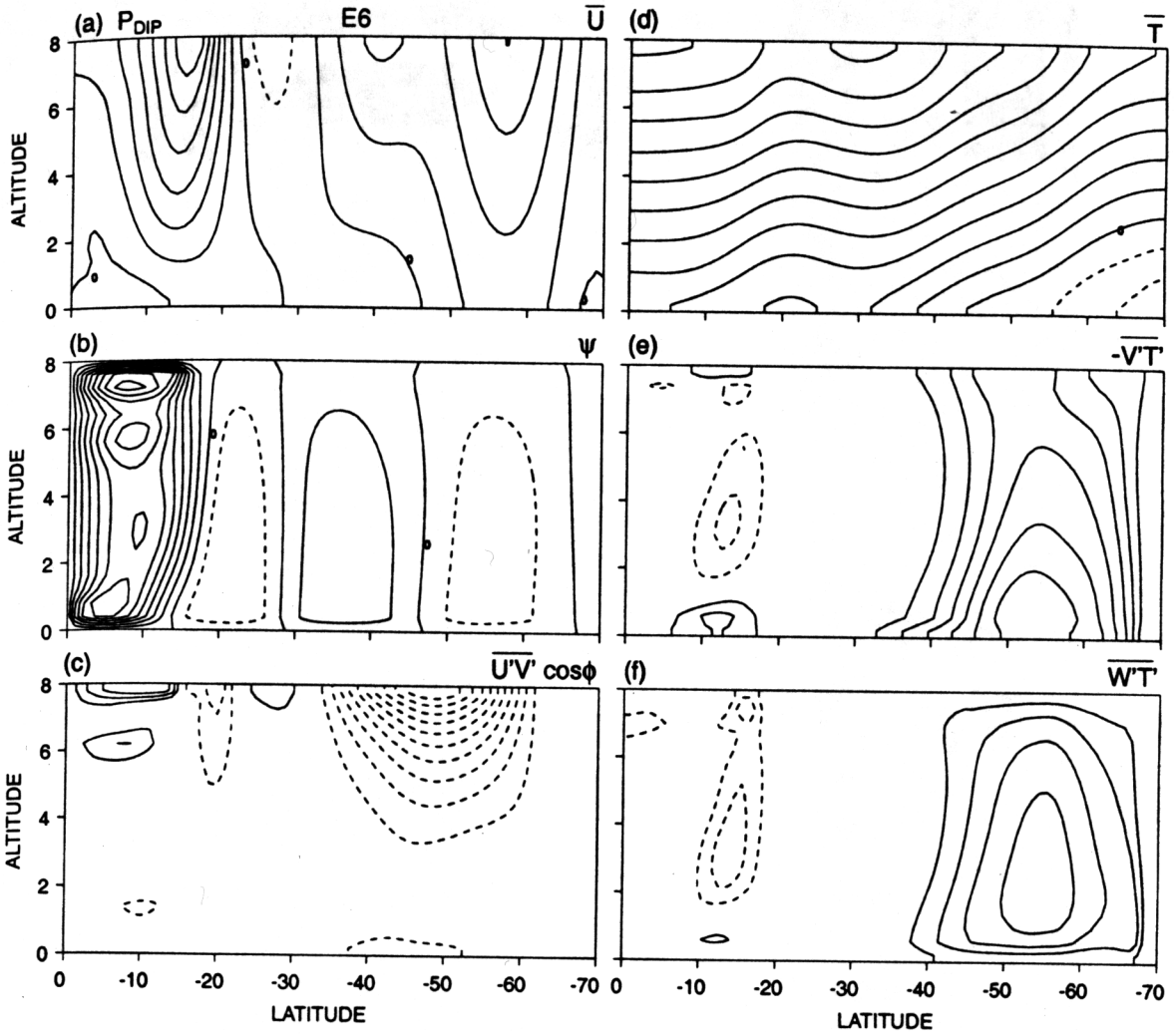

Fig. C6. Meridional sections of the primary fields and eddy transports for the terrestrial E6 case with double jets produced by an extra baroclinicity in low latitudes. The means are based on daily averages taken over 800–1000 days. In order, the contour interval, maximum and minimum values are (a) $(5, 35, -8)$ m s^{-1}; (b) $(1, 9.5, -2.0) \times 10^2$ m^2 s^{-1}; (c) $(1, 3.9, -10.8)$ m^2 s^{-2}; (d) $(4, 45, -11)$°C; (e) $(0.5, 3.5, -1.1)$°C m s^{-1}; (f) $(0.5, 2.3, -1.4) \times 10^{-3}$°C m s^{-1}. The zero-value contours are omitted for the eddy fields.

5. Multiple steady jets

To examine the transition between thin and thick 3-D flows, jovian parameters are used so that the more general multi-jet regime can be considered. In a related study, Part III, the dynamical response of very thin atmospheric layers was examined to see how multiple jets can be generated and maintained by a heating that produces a flow with either a highly-confined linear (LIN), or exponential (EXP), vertical structure. The jets were driven by the baroclinic instabilities that arise in response to latitudinal heating distributions having a variety of global and local components. The calculations showed that jets resembling the main jovian ones in amplitude, scale, and form can be generated and maintained in a steady configuration when the flow has the LIN structure. When the flow has the EXP structure, however, the jets migrate slowly but continuously equatorward while being regenerated in higher

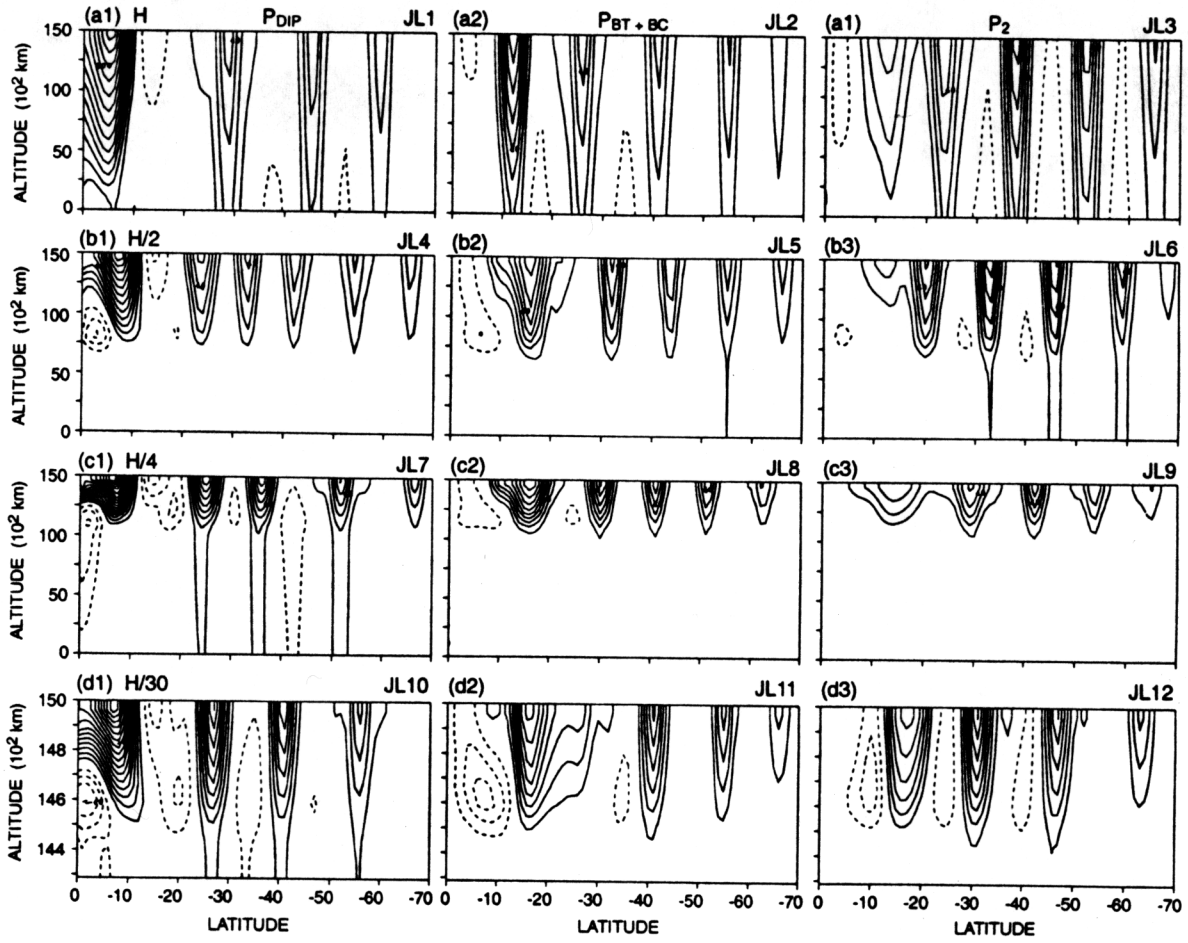

Fig. D1. Meridional zonal velocity sections for the jovian LIN cases, JL1–JL12, with different heating thicknesses and latitudinal profiles. The contour interval equals 10 m s^{-1} for all, while the maximum and minimum values and daily averaging intervals are (a1) $(134, -19)$ m s^{-1}, 9900–10000 days; (a2) $(79, -15)$ m s^{-1}, 3400–3500 days; (a3) $(65, -18)$ m s^{-1}, 1400–1500 days; (b1) $(126, -31)$ m s^{-1}, 1400–1500 days; (b2) $(75, -20)$ m s^{-1}, 1900–2000 days; (b3) $(66, -13)$ m s^{-1}, 1400–1500 days; (c1) $(176, -34)$ m s^{-1}, 2800–3000 days; (c2) $(97, -18)$ m s^{-1}, 2400–2500 days; (c3) $(58, -9)$ m s^{-1}, 1400–1500 days; (d1) $(166, -41)$ m s^{-1}, 6900–7000 days; (d2) $(83, -34)$ m s^{-1}, 1450–1500 days; (d3) $(81, -25)$ m s^{-1}, 3950–4000 days. The zero-value contours are omitted.

latitudes. For both structures, the flow is sensitive to the heating distribution in low latitudes where jets form only if a significant baroclinicity exists in that region; however, the barotropic instability associated with the W_1 jets can generate a superrotating current at the equator.

Now we first examine the transitions for flows with a LIN structure, and then in section 6 for flows with an EXP structure, with both vertical forms having confinement rates that go from low to high.

5.1 *The LIN range*

To illustrate the range of possible states of systems with the LIN structure, consider the solutions for four depths, $h = (H, H/2, H/4, H/30)$ and three heating profiles, $P(\phi) = (P_{DIP}, P_{BT+BC}, P_2)$, in Fig. D1 and Table D1. The $P_2(\phi)$ profile gives the *basic* circulation, while P_{BT+BC} modifies the extent of the barotropic and baroclinic zones in low and middle latitudes, as in Fig. 2. The P_{DIP} heating adds a second baroclinic component to produce a jet in low latitudes whose barotropic instability in

Table D1. The basic parameters for the jovian LIN cases in Figs. D1–D4. The P_{DIP} heating has $g(10°, 4°, -0.25)$ to define the center, half-width, and amplitude of the Gaussian cooling dip that is imposed upon a P_{BT+BC} component. The P_{BT+BC} heating is barotropic with a value of unity from the equator to $\phi = 6°$ (or 10° when it underlies the P_{DIP} cases), then baroclinic until vanishing at 70°. The thin structure has $S_1 = C[1, 0]$ and $S_2 = C[z_c^2, 0]$, while the thick2 has an exceptional form $S_2 = z'^2$. The heating rate has $\tau = 300$ days. The heating amplitudes, ΔT and δT, have °C units. The ν_4 coefficient varies about -10^{16} m^4 s^{-1}, while ν_2 goes from 0.01×10^4 to 2×10^4 m^2 s^{-1} as the flows become deeper. The horizontal grids have $\Delta\lambda = 1°$ over a 60° domain, and $\Delta\phi = 1°$ over 70°, except when $\Delta\phi = 0.5°$ for JL7. The vertical grid is uniform with $KZ = 20$, but uses a split form when $h' = 1/30$. The *time* column gives the extent of each calculation in units of 10^3 days, while τ_D is in days.

Case	h'	ΔT	δT	$P(\phi)$	$S(z)$	τ_D	time
JL1	1	0.1	0.1	P_{DIP}	thick2	10	10
JL2	1	0.1	0.1	P_{BT+BC}	thick2	10	3.5
JL3	1	0.15	0.2	P_2	thick2	10	1.5
JL4	1/2	0.3	0.4	P_{DIP}	thin	10	1.5
JL5	1/2	0.3	0.4	P_{BT+BC}	thin	10	2
JL6	1/2	0.35	0.4	P_2	thin	10	1.5
JL7	1/4	0.8	0.6	P_{DIP}	thin	10	3
JL8	1/4	0.8	0.8	P_{BT+BC}	thin	10	2.5
JL9	1/4	0.8	1	P_2	thin	10	1.5
JL10	1/30	6	4	P_{DIP}	thin	300	7
JL11	1/30	6	4	P_{BT+BC}	thin	30	1.5
JL12	1/30	6	4	P_2	thin	30	1.5

turn generates a superrotation at the equator, thus developing a *realistic* (Jupiter-like) circulation. The heating amplitudes are scaled so as to keep the zonal velocities within the same range for the various thicknesses, thereby allowing all the solutions to be plotted with the same contour interval in Fig. D1.

The top row of the figure shows that 4 or 5 jets can form in a thick layer for the chosen parameter range and $P(\phi)$ profiles. All of the jets have roughly the same width but display a variety of amplitude distributions. In the *basic* JL3 case, the strongest jets, W_3 and W_4, form in midlatitudes. But the redistribution of the heating by the P_{BT+BC} profile in the JL2 case increases the baroclinicity in low latitudes and results in W_1 becoming the strongest jet, though it is still centered at the same latitude, 12°, as before. To get jets to form in even lower latitudes requires the existence of the second baroclinic component of the P_{DIP} heating. In the JL1 case, this produces a W_1 jet strong enough and near enough to the equator that the eddies from the barotropic instability of its equatorward side can drive a superrotating westerly, W_0, of 134 m s^{-1} at the equator.

When the thickness is halved to $h = H/2$ and then again to $h = H/4$, in rows 2 and 3 of Fig. D1, the jets retain the same pattern of behavior as in the thick case, being 5 in number in most solutions. The very thin flows with $h \approx H/30$ also have the same character but differ in that they are derived using a split grid in the vertical. The form of the circulation thus appears to be independent of the layer's depth for the LIN structure, provided the parameters are scaled

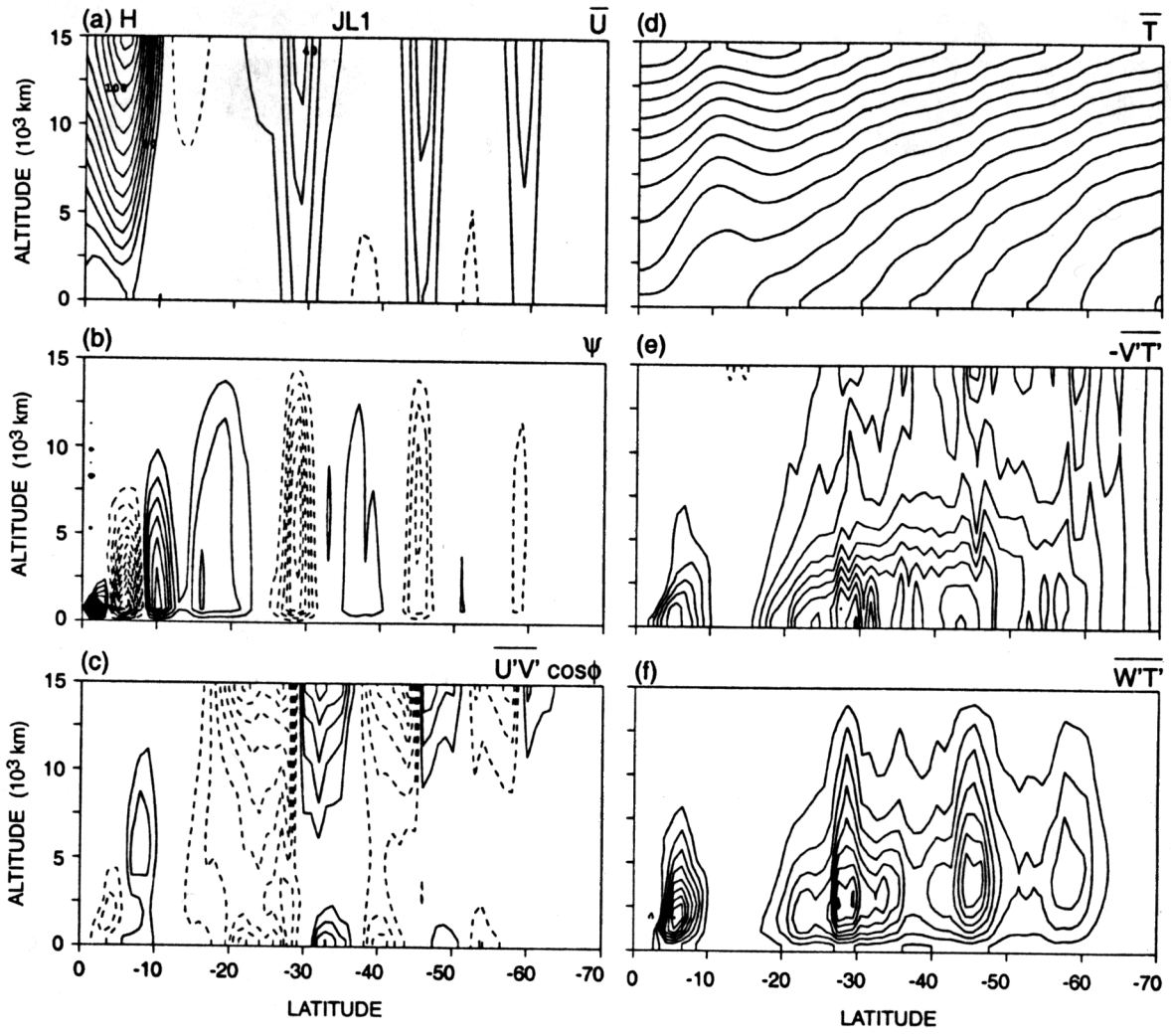

Fig. D2. Meridional sections of the primary fields and eddy transports for the jovian LIN case JL1, a thick system. The means are based on daily averages taken over 9900–10000 days. In order, the contour interval, maximum and minimum values are (a) $(10, 134, -19)$ m s^{-1}; (b) $(2, 20.1, -26.3) \times 10^4$ m^2 s^{-1}; (c) $(2, 11.2, -18.1)$ m^2 s^{-2}; (d) $(1, 19, -1) \times 10^{-2}$°C; (e) $(0.5, 5.6, -0.6) \times 10^{-3}$°C m s^{-1}; (f) $(1, 9.2, -1.4) \times 10^{-4}$°C m s^{-1}. The zero-value contours are omitted for the eddy fields.

appropriately. This raises an important question: if the jet width is independent of h, what dynamical processes determine it? To see how the dynamics actually varies with the thickness of the active layer, three cases, JL1, JL4 and JL10, are examined in detail. They represent the *realistic* circulation for layers that are thick, transitional, and thin, respectively.

5.2 *Thick LIN dynamics*

In the JL1 system, the axisymmetric spinup produces a broad westerly flow in midlatitudes and, thanks to the Gaussian cooling dip, a sharp westerly jet at 8°, with a weak easterly flow in between. Once perturbed, the broad westerly soon develops baroclinic instabilities that change it completely into three midlatitude westerly jets, Fig. D2a. The sharp axisymmetric component, however, survives in a modified form as a W_1 jet whose barotropic instability helps generate the westerly at the equator. An indirect cell is associated with each jet, with the one in the W_1 westerly being particularly strong and shallow. The direct cells all

lie within the weak intervening easterlies so there is no real Hadley cell at the equator.

The JL1 eddy transports in Fig. D2 reflect the action of four sets of nonlinear baroclinic instabilities, all centered on the cores of the W_{1-4} jets that they sustain near $\phi = (8, 28, 45, 60)°$. All transports have the same form within each jet: (a) a strong upward heat flux, $\overline{w'T'}$; (b) a distinct poleward heat flux, $-\overline{v'T'}$, that is strongest near the bottom surface and generates the planetary waves that propagate upward and then outward, both north and south; and, (c) an eddy momentum flux, $\overline{u'v'}$, created by these waves that converges on each jet core, mainly in the upper half. Although the $\overline{v'T'}$ flux peaks within the jets, it remains continuous as it relays the heat poleward across the easterlies at low levels—the EXP system differs in this regard. But in low latitudes the dynamics are somewhat different as the eddy momentum flux that drives the equatorial westerly is produced by a weak barotropic instability and does not show fully in Fig. D2c—such fluxes are discussed in detail in Williams (2003a,b).

5.3 *Transitional and thin LIN dynamics*

When the heating is restricted to the upper half of the fluid, as in the transitional JL4 case in Fig. D3, six westerly jets, W_{1-6}, plus an equatorial westerly current, W_0, form whose dynamics are similar to that of the thick JL1 flow, despite being vertically limited. The Ferrel cells remain deep and dominate the meridional flow except at the equator where a strong, vertically-bimodal Hadley cell forms. The jets all have the same width but different amplitudes; the lateral scale seems to be fixed in a process that is free to determine the amplitude. This differs from β turbulence theory where a preordained eddy energy level determines the lateral jet scale. Thin layer flows also differ from thick ones by having a weaker barotropic component, and a dominant first baroclinic mode.

However, according to the eddy fluxes, the baroclinic instability in a confined layer with the LIN structure does not differ in any fundamental way from the classical form seen in the thick case. Although confined aloft, the eddy momentum flux, $\overline{u'v'}$, still converges on the $W_{3,4,5}$ jet cores and traverses poleward across the $W_{2,6}$ jets, while a weak momentum flux traverses equatorward flux across the W_1 jet. The eddy heat fluxes are strongest just above the thermal interface in the jet cores, except in the W_1 westerly whose baroclinic instability is weak but whose barotropic instability is sufficient to drive the W_0 current at the equator. The eddies themselves, however, are equally strong in all six jets according to the kinetic energy field (not shown).

The flow in the really thin system with $h \approx H/30$, case JL10 in Fig. D4, is essentially just a more confined version of the previous example, and has been discussed in detail elsewhere (Williams 2003a), particularly as regards the eddy processes acting near the equator. The four jets and superrotation are accompanied by meridional cells that still reach the bottom surface[9] and are especially strong in low latitudes—their noisy component near the equator, probably related to deep waves generated below the interface, is excluded from the figure. In midlatitudes, the eddy heat fluxes again peak in the jet cores just above the interface, and generate the eddy momentum fluxes that converge on all the jet cores. In low latitudes, the baroclinic instability is weak but coexists with a barotropic instability capable of producing an equatorward eddy momentum flux that drives the W_0 current. This eddy flux occurs early in the flow evolution and is shown in Fig. 8 of Williams (2003a).

The eddy transports in all of the LIN cases, thick and thin, all resemble the fundamental forms seen in terrestrial GCMs with high rotation rates (Williams 1988), and all are associated with standard nonlinear baroclinic instabilities.

6. Multiple migrating jets

Consider now the circulations that are produced by a heating with the exponential (EXP) structure. A previous study, Part III, has shown that an EXP heating with a high confinement rate ($N = 200$) produces flows that are baroclinically unstable and lead to multiple jets. These jets migrate equatorward at a very slow rate (3 cm s^{-1}), and regenerate in high latitudes. To show that this behavior is typical,

9 The grid spacing Δz_2 is large near the bottom surface.

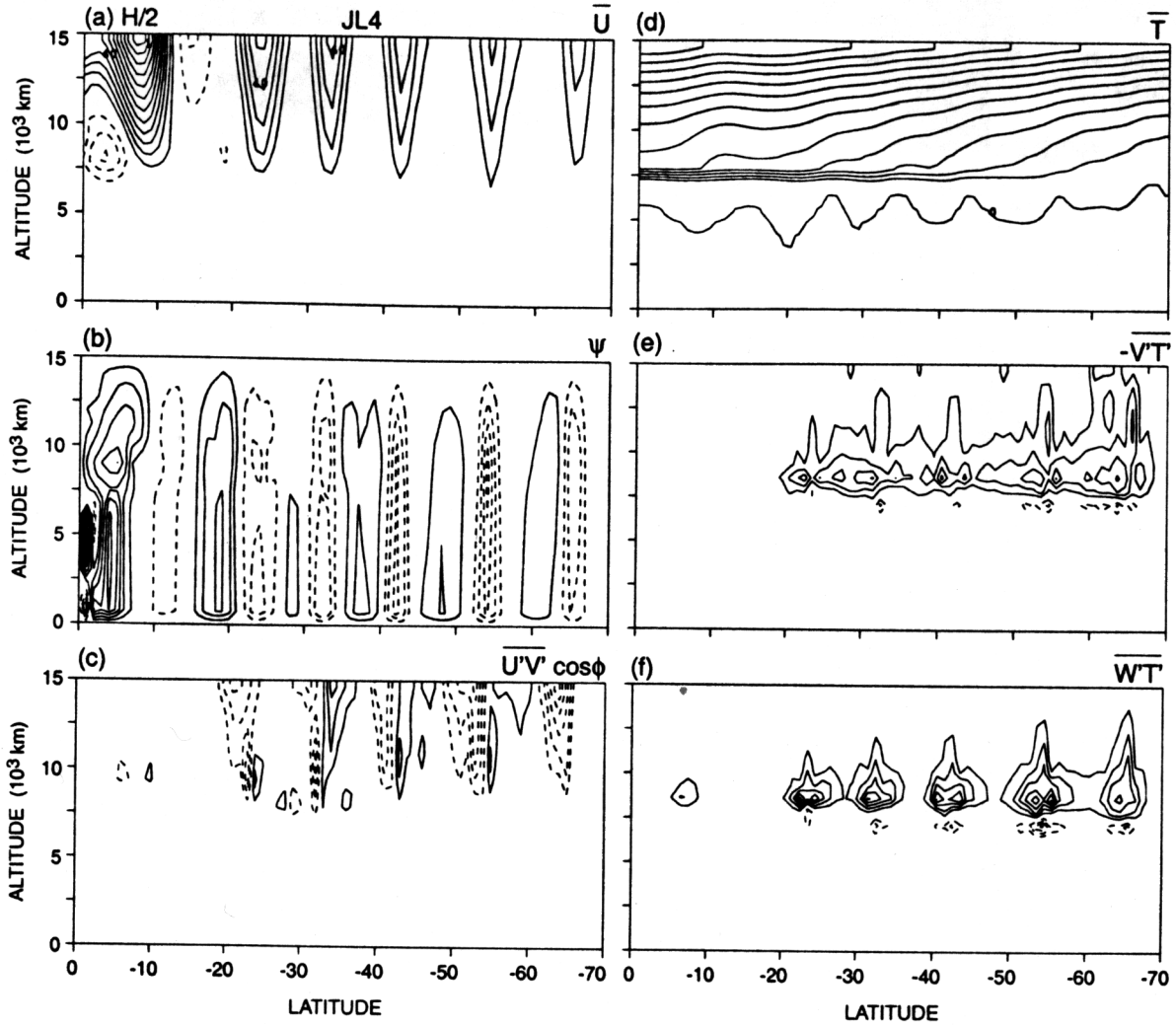

Fig. D3. Meridional sections of the primary fields and eddy transports for the jovian LIN case JL4, a transitional system. The means are based on daily averages taken over 1400–1500 days. In order, the contour interval, maximum and minimum values are (a) $(10, 126, -31)$ m s^{-1}; (b) $(5, 42.4, -30.5) \times 10^3$ m^2 s^{-1}; (c) $(1, 3.4, -6.0)$ m^2 s^{-2}; (d) $(5, 69, -0) \times 10^{-2}$°C; (e) $(1, 4.4, -2.3) \times 10^{-3}$°C m s^{-1}; (f) $(1, 6.1, -4.3) \times 10^{-4}$°C m s^{-1}. The zero-value contours are omitted for the eddy fields.

we now examine the EXP flows as they vary from thick to thin with confinement rates that go from $N = 0$ to $N = 200$.

6.1 *The EXP range*

To illustrate the transition from thick to thin, solutions are presented for the eight values of N shown in Fig. E1 and Table E1. The system with $N = 0$ is not strictly exponential as its heating has no vertical variation; it is in fact a simple case in which $u \sim z'$, and the background static stability vanishes—as in the axisymmetric EA4 case. In all cases only the fundamental $P_2(\phi)$ heating profile, with its single baroclinic zone, is used so any equatorial westerlies that arise do so from migration alone. All systems produce 4 or 5 jets as the heating amplitudes are all scaled so as to produce zonal velocities in the same fixed range.

As N increases, the jets leave the bottom surface, first in low latitudes at $N = 2$, then in midlatitudes at $N = 3$, and everywhere by $N = 5$. The form of the zonal velocity remains the same for $N = (5, 20, 200)$, with the jet am-

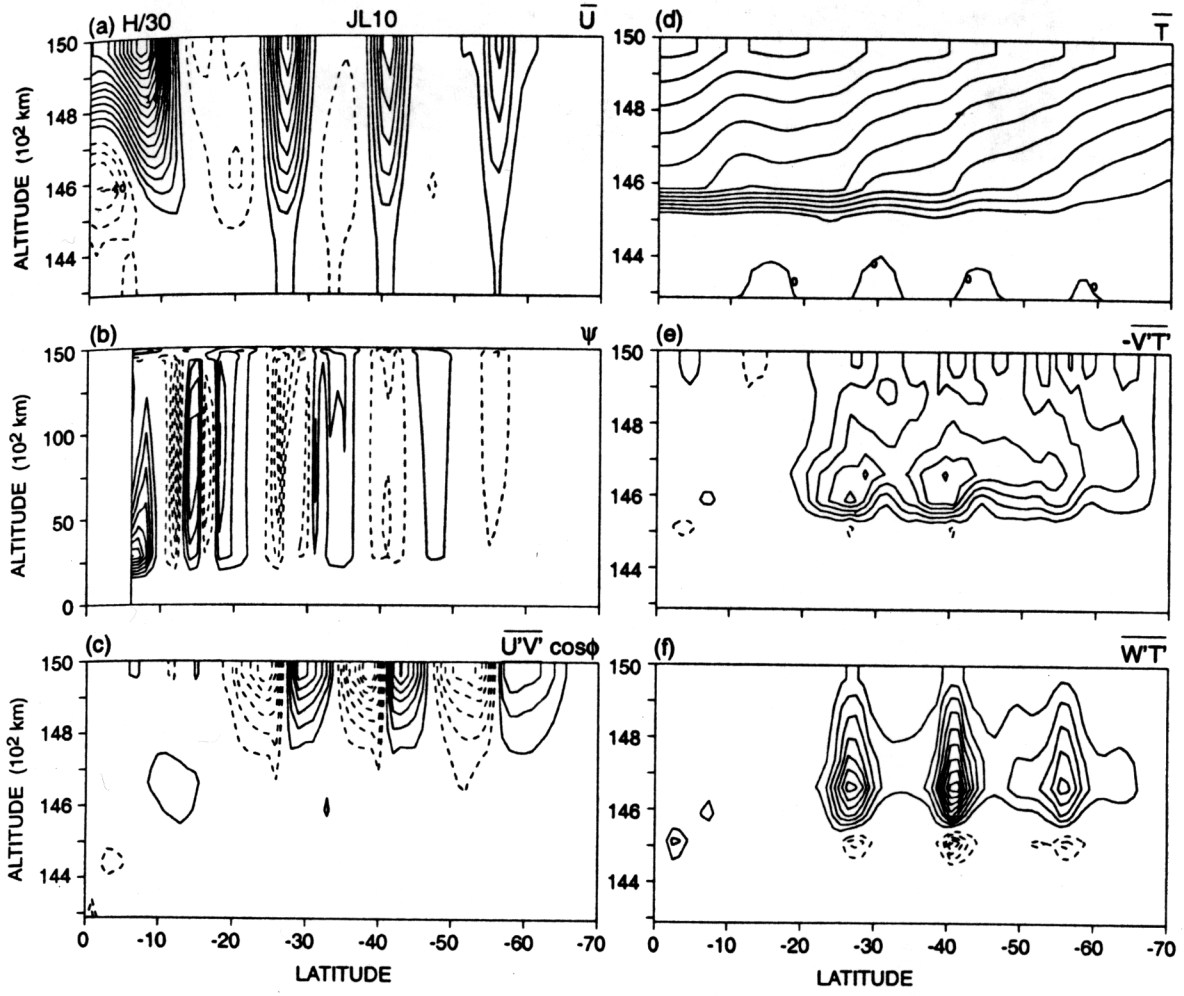

Fig. D4. Meridional sections of the primary fields and eddy transports for the jovian LIN case JL10, a thin system. The means are based on daily averages taken over 100–7000 days. In order, the contour interval, maximum and minimum values are (a) $(10, 166, -41)$ m s^{-1}; (b) $(1, 8.1, -5.3) \times 10^3$ m^2 s^{-1}; (c) $(2, 14.2, -17.9)$ m^2 s^{-2}; (d) $(0.8, 9.8, -0)$°C; (e) $(2, 12.4, -2.9) \times 10^{-2}$°C m s^{-1}; (f) $(2, 19.3, -10.7) \times 10^{-4}$°C m s^{-1}. The zero-value contours are omitted for the eddy fields. The streamfunction plot skips low latitudes.

plitudes decreasing poleward while the jet widths remain constant. The barotropic component cannot be behind the process controlling the jet scales as it becomes negligible as N increases. In the JE1 and JE2 cases, a westerly current also forms at the equator due to the migration of the W_1 jet; only these two cases were calculated long enough for this to be possible.

Nevertheless, in the EXP system the jets migrate at all N values. Figure E2 illustrates this for the two lengthy cases with $N = 0$ and 1, as well as for the unusual solution with $N = 2$. The JE1 solution for $N = 0$ contains a migration towards the equator even though the structure is not really exponential. In the JE2 case, the W_1 jet evolves quickly over the first 2000 days into an equatorial current that later merges with the migrating W_2 jet at 7000 days to produce the equatorial flow seen in Fig. E1b. Although migration is usually equatorward, it can on rare occasions be poleward, as for the JE3 case with $N = 2$ in Fig. E2c. In this example, the W_3 and W_4 jets move poleward while

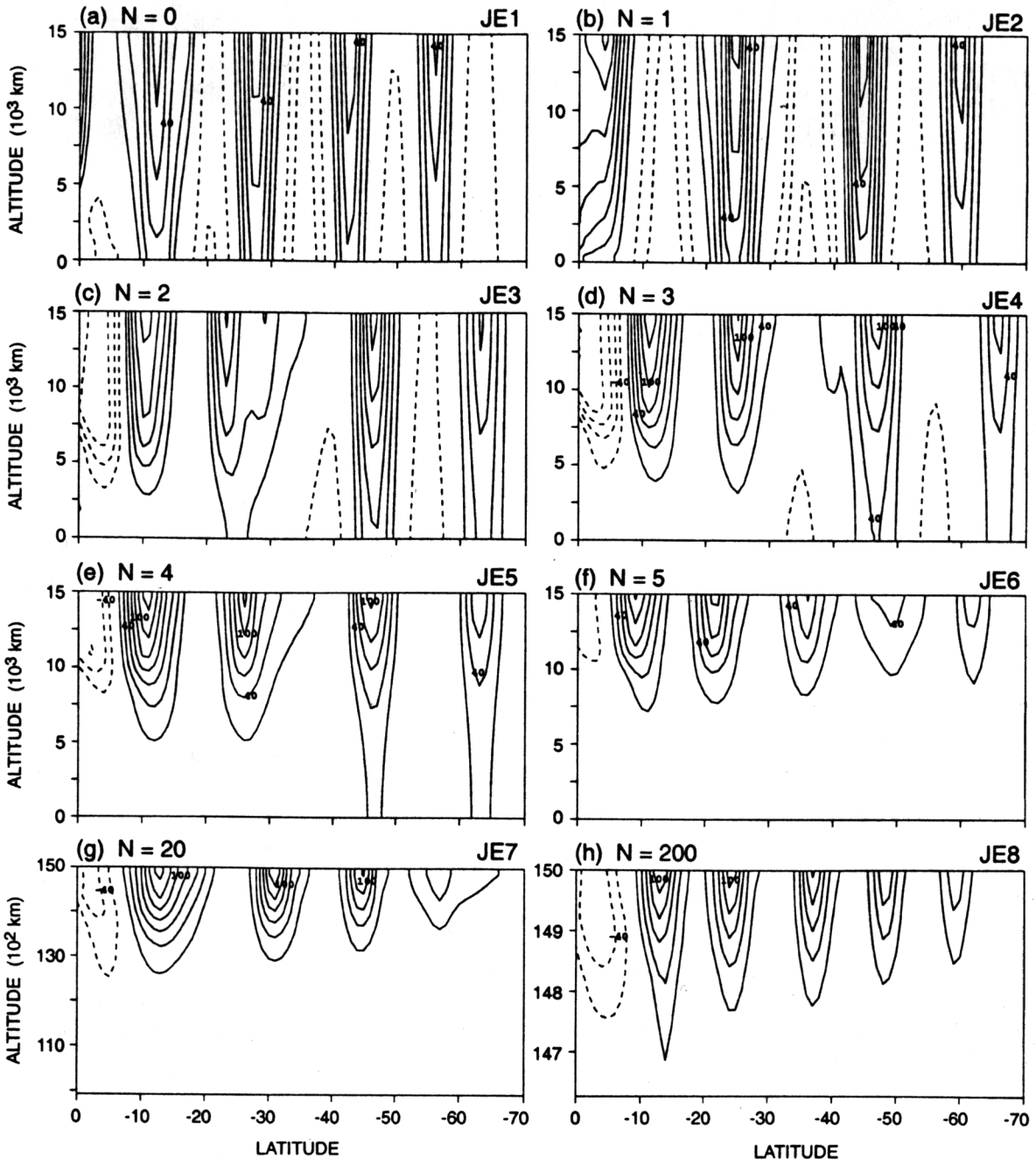

Fig. E1. Meridional zonal velocity sections for the jovian EXP cases, JE1–JE8, with different confinement rates, N. The means are based on daily averages over 9900–10000 days for (a)–(b), 1900–2000 days for (c)–(f), and 1950–2000 days for (g)–(h). In order, the contour interval, maximum and minimum values are (a) (10, 58, −26) m s^{-1}; (b) (10, 73, −32) m s^{-1}; (c) (15, 96, −57) m s^{-1}; (d) (20, 137, −91) m s^{-1}; (e) (20, 151, −61) m s^{-1}; (f) (20, 122, −33) m s^{-1}; (g) (20, 147, −49) m s^{-1}; (h) (20, 116, −57) m s^{-1}. The zero-value contours are omitted.

Table E1. The basic parameters for the jovian EXP cases in Figs. E1–E5. All cases have a $P_2(\phi)$ heating distribution. The structure goes as $S_1 = (d/dz)[\mathrm{sech}(Nz')]$ and $S_2 = \exp(Nz')$, which simplifies to $S_1 = 1$ and $S_2 = 0$ when $N = 0$. The heating and drag rates equal 300 and 10 days, respectively. The heating amplitudes, ΔT and δT, have °C units. The diffusion has $\nu_4 = -20 \times 10^{16}$ m^4 s^{-1} and $\nu_2 = 0$. The first five cases use a uniform grid, while for the next three Δz varies in turn as $\exp(\{1, 2, 7\}z')$, all with $KZ = 20$. The *time* column gives the extent of each calculation in units of 10^3 days.

Case	N	ΔT	δT	time
JE1	0	0.11	0	10
JE2	1	0.18	0.2	10
JE3	2	0.3	0.3	2
JE4	3	0.5	0.3	2
JE5	4	0.75	0.5	2
JE6	5	0.8	0.5	2
JE7	20	4	2	2
JE8	200	25	4	2

the W_1 and W_2 jets remain unusually steady. Other EXP cases with $N = 2$ have the more customary equatorward migration. But given the fact that the jets also migrate in the non-exponential JE1 case, we conclude that the migration is due to a common factor, one not shared with the LIN system, namely the weak static stability.[10]

To examine the range in the dynamics of the EXP flows, details are presented of the solutions at $N = (0, 3, 200)$ that represent the thick, transitional, and thin structures. Because of the migration, the eddy fluxes are defined using relatively short time intervals.

6.2 *Thick EXP dynamics*

In Fig. E3 for the thick JE1 case, with its exceptional but simple structure, the net static stability is positive and due entirely to the vertical heat transport by the eddies. The strong Hadley cell that forms at the equator also creates its own static stability. This vertical heat transport by the eddies, and by the Hadley cell corresponds to those seen earlier in the terrestrial E3 and EA4 solutions without a background static stability. The eddy-driven Ferrel cells are much stronger in low latitudes, though the instabilities themselves are weaker there. At the equator, the unusual narrow current is just the residual of a broader current that collapses at 6000 days under pressure from a migrating W_2 jet, Fig. E2a.

Although the multiple baroclinic instabilities are narrow, they remain deep, with the lateral heat flux, $\overline{v'T'}$, being unusually strong at all heights in the absence of a background static stability, Fig. E3e. This flux actually peaks between the jets and is discontinuous within the jet cores.[11] Such fluxes may be related to those produced by the inter-jet modes discussed by Lee (1997) for low-drag systems. This unusual variation differs from behavior in the LIN and classical systems and suggests that it may be responsible for the migration in the EXP system. The vertical eddy heat flux, however, peaks as usual in the jet cores, while the converging eddy momentum flux that drives the jets is confined to the upper third of the domain. Overall, the nonlinear baroclinic instabilities appear to have some novel characteristics in the absence of a background static stability, and appear to be capable of arising in latitudes as low as 15° for the $P_2(\phi)$ heating.

6.3 *Transitional and thin EXP dynamics*

In the transitional JE4 case in Fig. E4, two of the jets are detached from the bottom surface in low latitudes and coexist with the two that remain in touch with the surface in midlatitudes. The meridional cells are all deep but tend to be vertically bimodal and stronger aloft in low latitudes. The jets and cells form in response to baroclinic instabilities that are confined to the upper third of the fluid in low latitudes but are deep elsewhere. Thin and thick instabilities can easily coexist alongside each other.

The JE4 instabilities mostly occur in a layer that is nearly statically neutral, and over which the $\overline{v'T'}$ flux is vertically uniform and maximal between the jets. The $\overline{w'T'}$ flux appears to have double maxima within each jet and to be

10 Migrating cells and jets also exist in some axisymmetric systems (Satoh 1994, 1995).

11 This can be seen more easily in 1-D cross sections, such as in Fig. 14e of Williams (2003a).

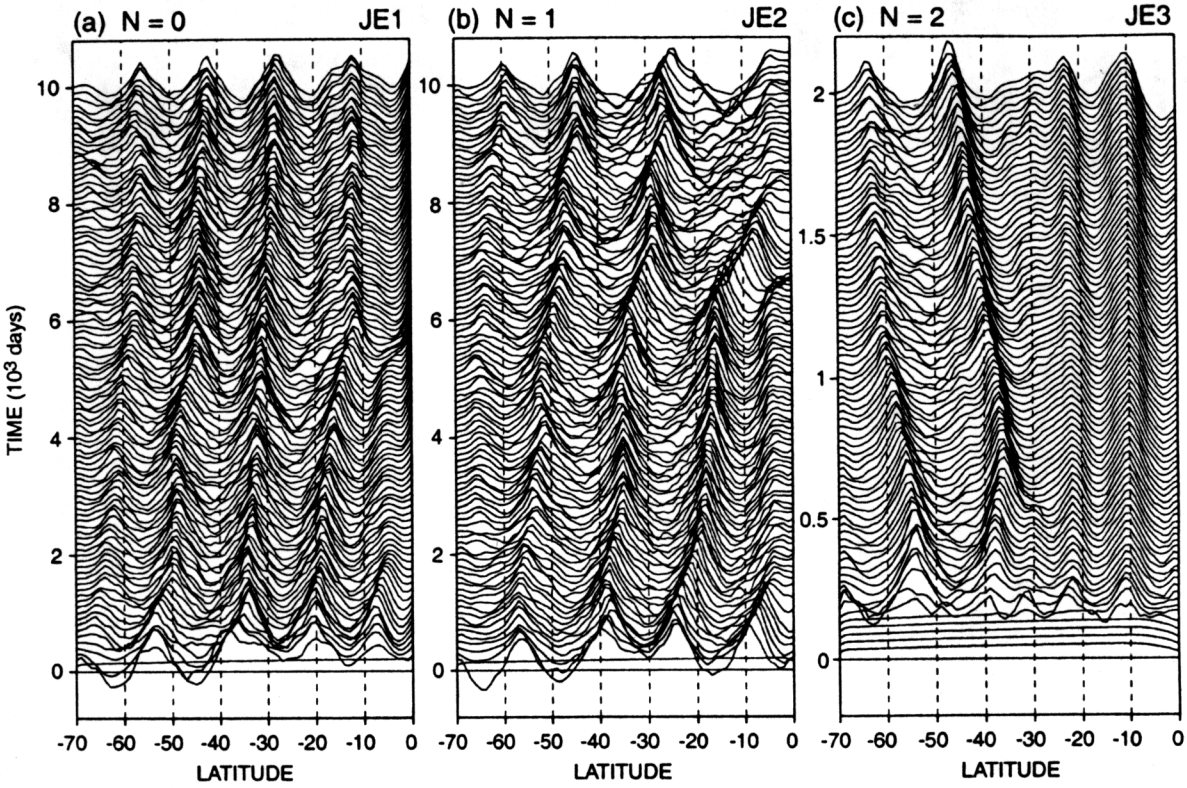

Fig. E2. Time sections of the mean zonal velocity sampled near the top surface for the jovian EXP cases with $N = 0, 1, 2$. Scales for the maximum $\bar{u}(\phi, t)$ are (a) 81 m s^{-1}, (b) 94 m s^{-1}, (c) 113 m s^{-1}, and all are equivalent to 8 times the vertical spacing between the curves.

broadly distributed, reflecting the existence of a novel form of baroclinic instability. On the other hand, the $\overline{u'v'}$ flux is confined to a very shallow layer ($h \approx H/6$) near the top surface, converging on the $W_{1,2,3}$ jets and traversing the W_4 jet.

Similar characteristics are seen when the flow is confined to a really thin layer in the final JE8 case in Fig. E5. The five jets are stronger and deeper towards low latitudes but their widths remain constant. The eddy momentum transport is confined to an even shallower surface layer, while the lateral eddy heat transport again peaks between the jets, and the vertical eddy heat flux again appears to have double maxima within each jet. The cells, however, still extend down to the bottom surface, where Δz is large. All of these features contain clues—as yet undeciphered—to the dynamical processes that lie behind the formation and maintenance of the jets.

Although they migrate, most EXP jets exhibit the classical eddy features associated with nonlinear baroclinic instabilities, even though all fluxes are confined to an upper layer that is close to having a neutral static stability in the thinner states. Such modes may be explainable by extending Fjortoft's (1951) advective theory—see section 2.4. Asymmetries in the converging $\overline{u'v'}$ fluxes within the jets, as well as the peaking of the $\overline{v'T'}$ fluxes between the jets, may be the cause of the migration and may be attributable to the particular character of the baroclinic instability and wave dispersion that exists in the EXP system. But the behavior does not depend on the confinement rate; migration and the same form of baroclinic instability occur at all values of N, from thin to thick.

7. Conclusions

The five sets of solutions discussed above help define the range of basic circulations that occur in thick, thin, and transitional systems. They lead to the following conclusions.

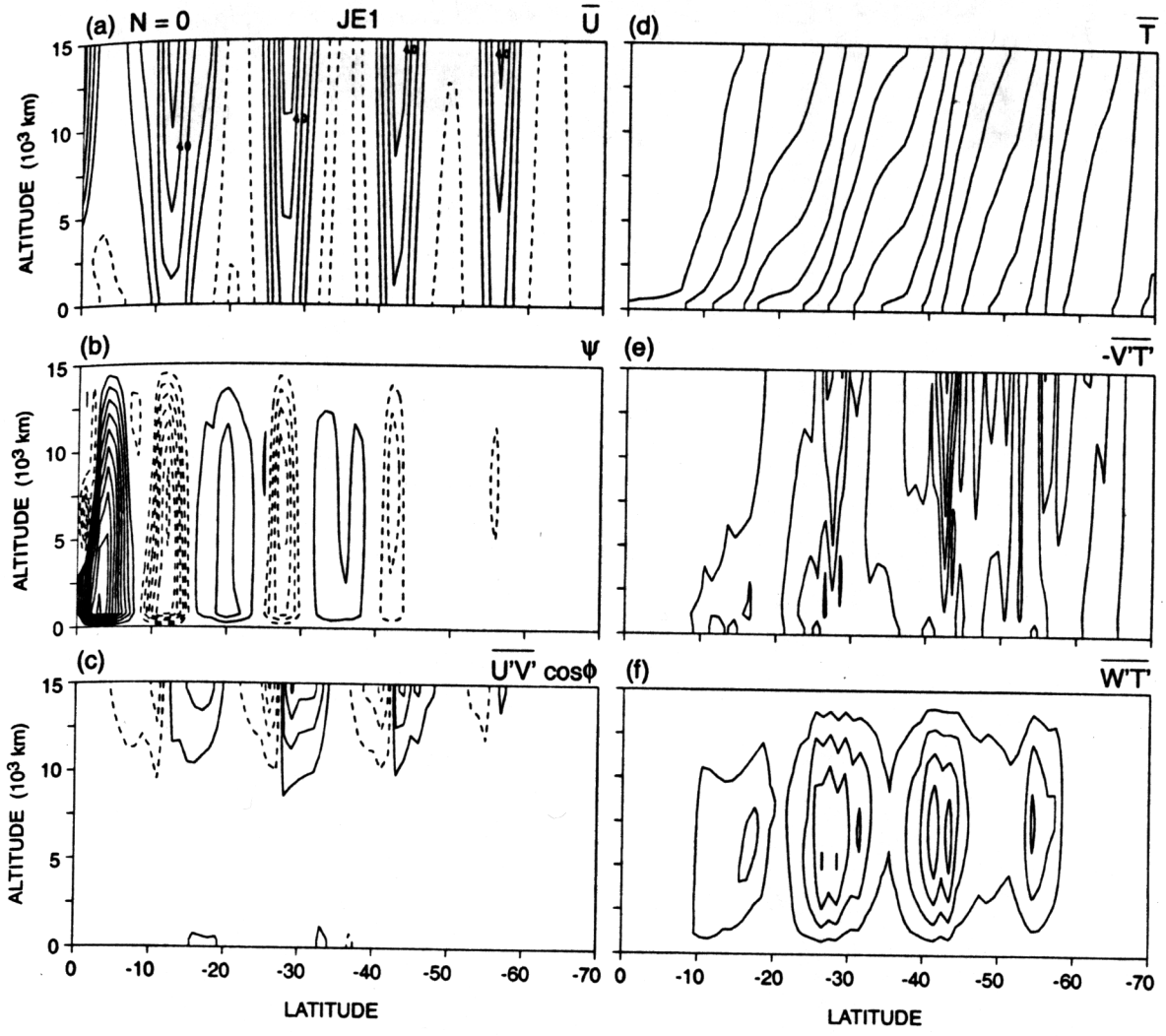

Fig. E3. Meridional sections of the primary fields and eddy transports for the jovian EXP case JE1, a thick system with $N = 0$. The means are based on daily averages taken over 9900–10000 days. In order, the contour interval, maximum and minimum values are (a) $(10, 58, -26)$ m s^{-1}; (b) $(10, 51.7, -36.4) \times 10^4$ m^2 s^{-1}; (c) $(10, 41.6, -41.4)$ m^2 s^{-2}; (d) $(0.5, 11, 2) \times 10^{-2}$°C; (e) $(1, 5.7, -0.7) \times 10^{-3}$°C m s^{-1}; (f) $(5, 23.4, -0.7) \times 10^{-4}$°C m s^{-1}. The zero-value contours are omitted for the eddy fields.

7.1 The terrestrial axisymmetric set

The terrestrial axisymmetric solutions show that the cells are wider, and the fronts sharper when the drag is reduced. The classical theory of Held and Hou (1980), and Satoh (1994), can be adapted to explain this behavior even though it cannot be extended to describe the complex interaction between the two zonal flow components, U_A and U_R. When the drag is absent completely, the degeneracy of the equations can be overcome by activating a horizontal diffusion; this allows a global thermal wind to emerge. Such a state is possible according to theory, but its realization is rare.

When the background static stability is set to zero, an orderly circulation still occurs and aspects of the theory still hold despite the greater nonlinearity and the violation of some consistency constraints. In particular, the Hadley cell still has the width expected from the theory even though it is now much stronger, tilted, and transports enough heat upward to create its own static stability. Furthermore, the U_A and U_R zonal winds still occur but merge dif-

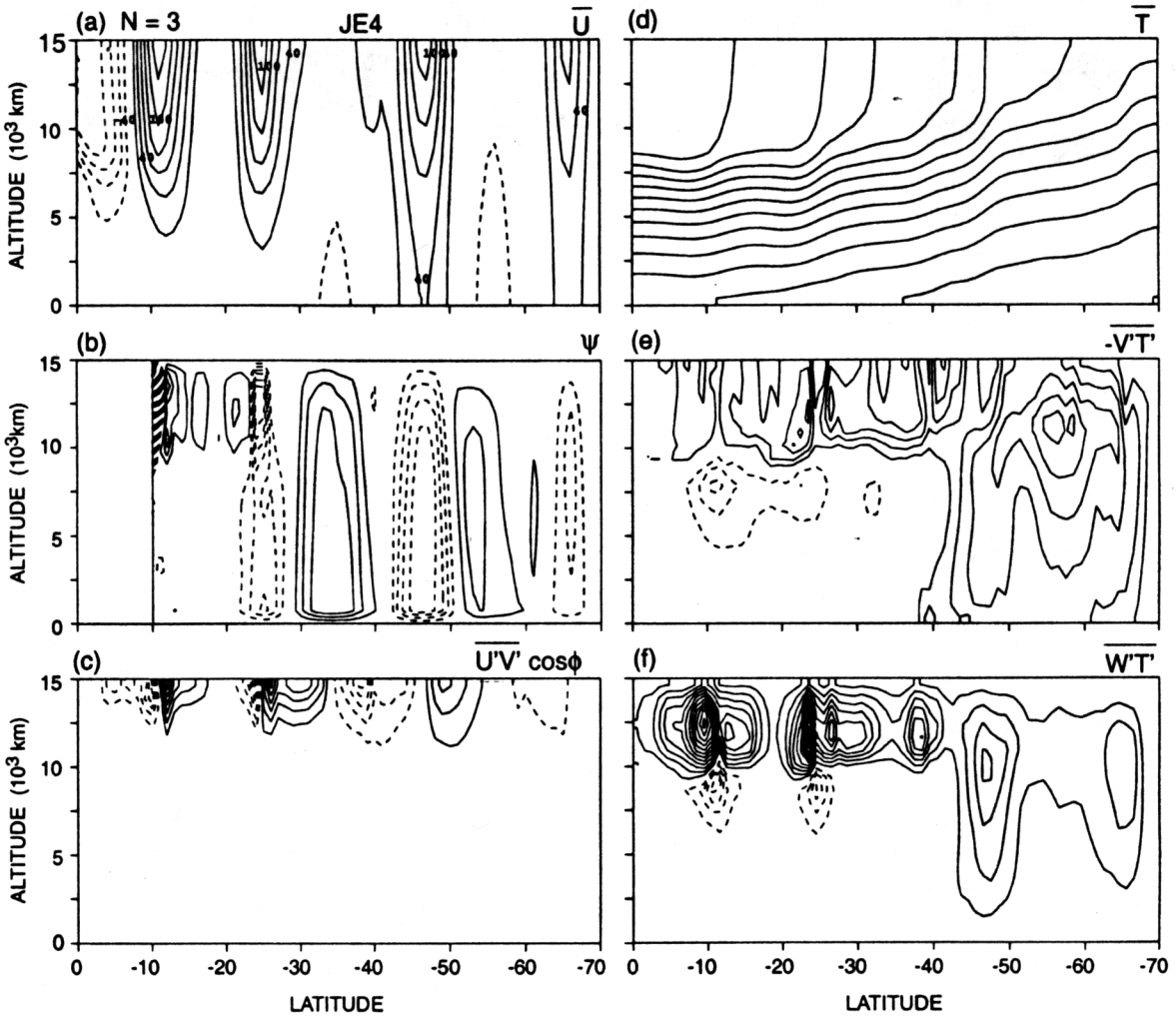

Fig. E4. Meridional sections of the primary fields and eddy transports for the jovian EXP case JE4, a transitional system with $N = 3$. The means are based on daily averages taken over 1900–2000 days. In order, the contour interval, maximum and minimum values are (a) $(20, 137, -91)$ m s^{-1}; (b) $(2, 9.8, -6.8) \times 10^4$ m^2 s^{-1}; (c) $(10, 66, -66)$ m^2 s^{-2}; (d) $(4, 54, 4) \times 10^{-2}$°C; (e) $(3, 12.8, -6.6) \times 10^{-3}$°C m s^{-1}; (f) $(5, 62.5, -27.4) \times 10^{-4}$°C m s^{-1}. The zero-value contours are omitted for the eddy fields. The streamfunction plot skips low latitudes.

ferently. The theory applies beyond its formal limits so perhaps it could be extended to deal with a zero static stability.

The classical theory also remains valid in the high rotation limit, with the flow decreasing gradually and continuously towards extinction. The width of the Hadley cell, however, tends to be more than double the theoretical value when $\Omega^* > 15$ and $\phi_H < 3°$. At these scales, the theory's neglect of certain nonlinear terms is no longer valid.

7.2 *The jovian axisymmetric set*

The axisymmetric set with jovian parameters examines the various transitions that occur in the circulation form when changes are made in the rotation rate, vertical confinement, and heating profile. The solutions show that the classical theory applies best over the middle range of rotation rates. At low rates, the circulations contain thermal fronts, axisymmetric instabilities, and strong easterlies, features that are only partly described by the theories

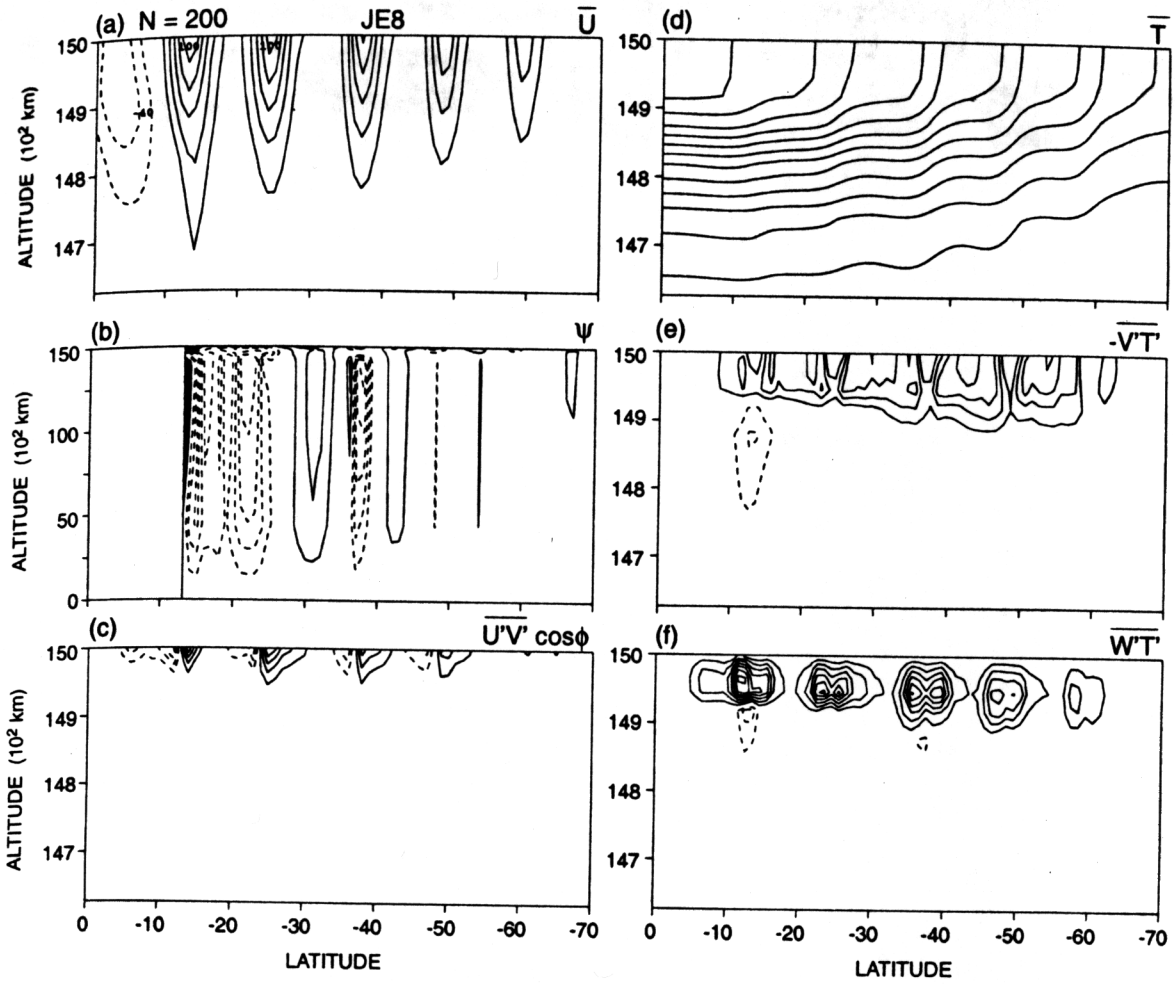

Fig. E5. Meridional sections of the primary fields and eddy transports for the jovian EXP case JE8, a thin system with $N = 200$. The means are based on daily averages taken over 1950–2000 days. In order, the contour interval, maximum and minimum values are (a) $(20, 116, -57)$ m s^{-1}; (b) $(5, 47.5, -36.8) \times 10^2$ m^2 s^{-1}; (c) $(20, 100, -82)$ m^2 s^{-2}; (d) $(2, 24, 0)$°C; (e) $(2, 10.0, -4.3) \times 10^{-1}$°C m s^{-1}; (f) $(1, 7.3, -2.6) \times 10^{-3}$°C m s^{-1}. The zero-value contours are omitted for the eddy fields. The streamfunction plot skips low latitudes.

of Schneider (1977), Held and Hou (1980), Satoh (1994), and Fang and Tung (1996). At high rates, the Hadley cell no longer slopes, the meshing of the U_A and U_R winds no longer produces a second peak in the zonal flow, and the temperature no longer deviates much from the radiative distribution.

The circulations in thick and thin axisymmetric flows are similar to each other so the transition between them is gradual and continuous. The thin system still contains the U_A and U_R winds, and the Hadley cell has the usual width even though it is vertically bimodal and stronger aloft. The classical theory could be adapted to describe such systems. The location of the Hadley cell, however, depends on the latitudinal heating profile and arises at the interface between the baroclinic and barotropic regions; it is displaced from the equator when the barotropic zone is wider than the cell.

7.3 *The basic terrestrial set*

The basic 3-D terrestrial circulations can take on a variety of related forms. The jet location and cell width, in particular, depend on the amplitude of the heating as much as on its dis-

tribution. Consequently, the jets are restricted under the $P_2(\phi)$ heating profile to certain latitudes between 30° and 50°. In the absence of a background static stability, a form of baroclinic instability, one not described by existing theory, arises and stabilizes the system by transporting heat upwards in midlatitudes, while a stronger Hadley cell does likewise in low latitudes.

When the surface drag is weak, the flow develops a stronger barotropic component that eventually acts to suppress the baroclinic instability. A weak instability still occurs, but is confined to a shallow layer near the ground, with peaks in low and high latitudes rather than in midlatitudes. The nature of the baroclinic instability also alters when double jets are created in each hemisphere. These occur when the rotation rate is quadrupled or when a second source of baroclinicity is introduced in low latitudes. In the high rotation case, the eddies and waves have a smaller lateral scale and tend to converge momentum into the jet cores, rather than transport it poleward across the jet as in the high-baroclinicity control case. On the other hand, adding baroclinicity in low latitudes produces a near-axisymmetric flow near the equator that coexists with the usual, control-like, eddy-driven jet, now located in higher latitudes. Such low-latitude jets can also be barotropically unstable, and thence drive superrotating westerlies at the equator.

7.4 *The jovian LIN set*

For the 3-D system with jovian parameters and the confined linear (LIN) heating structure, four or five jets usually form regardless of how deep the heated layer is—provided that the heating amplitude is scaled to keep the velocities within the same range. The jets tend to have the same width as each other but their amplitudes vary, with the strongest usually occurring in midlatitudes. If the baroclinicity is boosted in low latitudes, stronger jets form whose barotropic instability can drive a superrotation at the equator, for any layer thickness. The meridional circulations are usually dominated by the Ferrel cells and they always reach the bottom surface regardless of the thickness of the jets, perhaps in keeping with the "downward control" theory of Haynes et al. (1991), even though the model is Boussinesq. The eddies always converge momentum into the cores of the multiple jets. Thus the thin and thick layers appear to have a common dynamics, with the confined layers exhibiting the classical modes when created under the LIN formulation.

7.5 *The jovian EXP set*

Similarly, the 3-D system with the confined exponential (EXP) heating structure also develops four or five jets, regardless of the confinement rate (over $N = 0$–200), provided the heating amplitude is scaled appropriately. In most cases the jets migrate slowly towards the equator and regenerate in high latitudes, although poleward migration is also possible. The limiting case with $N = 0$ is not exponential but it does have migrating jets; this suggests that the migration occurs in any system that has a weak static stability.

The baroclinic instabilities that occur within such near-neutral layers produce a very shallow momentum convergence into the jet cores. They also produce lateral eddy heat fluxes that peak *between* the jets and almost vanish within the jet cores. The inter-jet modes of Lee (1997) may help explain why this pattern of heat transfer occurs but no theory as yet proves that it contributes to the jet migration. Nor does it explain why the jets again have a constant width but varying amplitudes.

As the heating becomes more confined aloft, the jets detach from the bottom surface, first in low latitudes when $N = 2$, then in midlatitudes when $N = 5$. At higher confinement rates, the jets tend to be deeper towards the equator even though the baroclinic instabilities are deeper towards the pole. Equatorial westerlies can arise either through migration or by boosting the baroclinicity to give barotropically unstable jets in lower latitudes.

7.6 *Implications*

The above axisymmetric solutions indicate that the classical theory of Held and Hou (1980) also applies reasonably well to cases that violate its formal constraints. Furthermore, they suggest that the theory could be extended to describe systems with no static stability and to explain flows confined to thin layers. Explanation of the behavior at high rotation rates only needs a minor improvement. The solstitial

states remain, however, as a much needed generalization.

Baroclinic instability theory needs to be extended to explain the forms that occur when (a) there is no static stability, and when (b) the drag is so weak, the barotropic component tends to suppress the eddies. How the instabilities and other processes form multiple jets in thick or thin systems and determine the latitudinal scale is not well understood. As discussed elsewhere in section 2.4, the β turbulence cascades that are usually invoked to explain jet formation (Rhines 1975) do not seem to apply as well to thin layers. Jets in thin and thick systems have the same lateral scale even though the barotropic component varies from weak to strong; this suggests that the scale is determined primarily by baroclinic processes.

Jet migration is a novel phenomenon that lacks any theoretical underpinnings. It seems to be a byproduct of the form of baroclinic instability that occurs when the static stability is weak aloft. Understanding why the poleward eddy heat fluxes peak between the jets and vanish within them, and why the eddy momentum fluxes converge asymmetrically into the jet cores, may explain why the jets migrate. Perhaps novel nonlinear modes occur in the exponential structures or maybe the migration towards the equator is just the ultimate cascade of energy towards larger scales?

In an earlier paper (Williams 1988), the basic parameters of a general circulation model were varied to help define the dynamical range of global circulations and to try to isolate the basic elements involved in the various states. That study is extended here to see if there are two limiting classes of circulation, one for thick layers and another for thin. However, we find that the circulations in confined layers are just variations on the basic thick forms that were documented earlier; only the jet migration is really novel. Although the processes involved may be few in number, they are rich in form and produce a wide range of circulations.

Acknowledgments

Thanks go to Geoffrey Vallis and the Reviewers for perceptive comments that helped improve this paper, and to Catherine Raphael for organizing the graphics.

References

Benilov, E.S., 1995: Baroclinic instability of quasi-geostrophic flows localized in a thin layer. *J. Fluid Mech.*, **288**, 175–199.

Bryan, K., 1969: A numerical method for the study of the circulation of the World Ocean. *J. Comput. Phys.*, **4**, 347–376.

Cho, J.Y.-K. and L.M. Polvani, 1996: The emergence of jets and vortices in freely evolving, shallow-water turbulence on a sphere. *Phys. Fluids*, **8**, 1531–1552.

Edmon, H.J., B.J. Hoskins and M.E. McIntyre, 1980: Eliassen-Palm cross-sections for the troposphere. *J. Atmos. Sci.*, **37**, 2600–2616.

Fjortoft, R., 1951: Stability properties of large-scale atmospheric disturbances. *Compendium of Meteorology. Amer. Meteor. Soc.*, 454–462.

Fang, M. and K.K. Tung, 1996: A simple model of nonlinear Hadley circulation with an ITCZ: Analytical and numerical solutions. *J. Atmos. Sci.*, **53**, 1241–1261.

Gill, A.E., J.S.A. Green and A.J. Simmons, 1974: Energy partition in the large-scale ocean circulation and the production of mid-ocean eddies. *Deep-Sea Res.*, **21**, 499–528.

Haynes, P.H., C.J. Marks, M.E. McIntyre, T.G. Shepherd and K.P. Shine, 1991: On the "downward control" of extratropical diabatic circulations by eddy-induced mean zonal forces. *J. Atmos. Sci.*, **48**, 651–678.

Held, I.M. and A.Y. Hou, 1980: Nonlinear axially symmetric circulations in a nearly inviscid atmosphere. *J. Atmos. Sci.*, **37**, 515–533.

——— and B.J. Hoskins, 1985: Large-scale eddies and the general circulation of the troposphere. *Advances in Geophysics*, Vol. 28A, Academic Press, 3–31.

Huang, H.-P. and W.A. Robinson, 1998: Two-dimensional turbulence and persistent zonal jets in a global barotropic model. *J. Atmos. Sci.*, **55**, 611–632.

———, B. Galperin and S. Sukoriansky, 2001: Anisotropic spectra in two-dimensional turbulence on the surface of a rotating sphere. *Phys. Fluids*, **13**, 225–240.

James, I.N., 1987: Suppression of baroclinic instability in horizontally sheared flows. *J. Atmos. Sci.*, **44**, 3710–3720.

——— and L.J. Gray, 1986: Concerning the effect of surface drag on the circulation of a baroclinic planetary atmosphere. *Quart. J. Roy. Meteor. Soc.*, **112**, 1231–1250.

Killworth, P.D., 1980: Barotropic and baroclinic instability in rotating stratified fluids. *Dyn. Atmos. Oceans*, **4**, 143–184.

Lee, S., 1997: Maintenance of multiple jets in a

baroclinic flow. *J. Atmos. Sci.*, **54**, 1726–1738.

Panetta, R.L., 1993: Zonal jets in wide baroclinically unstable regions: Persistance and scale selection. *J. Atmos. Sci.*, **50**, 2073–2106.

Rhines, P.B., 1975: Waves and turbulence on a beta plane. *J. Fluid Mech.*, **69**, 417–443.

———, 1977: The dynamics of unsteady currents. *The Sea*, **Vol. 6**, E.D. Goldberg, J.N. McCave, J.J. O'Brien and J.H. Steele, Eds., Wiley, 189–318.

———, 1994: Jets. *Chaos*, **4**, 313–339.

Salmon, R., 1998: *Lectures in Geophysical Fluid Dynamics*. Oxford University Press, 378 pp.

Saravanan, R., 1993: Equatorial superrotation and maintenance of the general circulation in two-level models. *J. Atmos. Sci.*, **50**, 1211–1227.

Satoh, M., 1994: Hadley circulations in radiative-convective equilibrium in an axially symmetric atmosphere. *J. Atmos. Sci.*, **51**, 1947–1968.

———, 1995: Hadley circulations and large-scale motions of moist convection in the two-dimensional numerical model. *J. Meteor. Soc. Japan*, **73**, 1059–1078.

Schneider, E.K., 1977: Axially symmetric steady-state models of the basic state for instability and climate studies. Part II: Nonlinear calculations. *J. Atmos. Sci.*, **34**, 280–297.

Simmons, A.J. and B.J. Hoskins, 1978: The life cycles of some nonlinear baroclinic waves. *J. Atmos. Sci.*, **35**, 414–432.

Smagorinsky, J., 1963: General circulation experiments with the primitive equations. 1. The basic experiment. *Mon. Wea. Rev.*, **91**, 99–164.

Suarez, M.J. and D.G. Duffy, 1992: Terrestrial superrotation: A bifurcation of the general circulation. *J. Atmos. Sci.*, **49**, 1541–1554.

Treguier, A.M. and R.L. Panetta, 1994: Multiple zonal jets in a quasigeostrophic model of the Antarctic circumpolar current. *J. Phys. Oceanogr.*, **24**, 2263–2277.

Vallis, G.K. and M.E. Maltrud, 1993: Generation of mean flows and jets on a beta plane and over topography. *J. Phys. Oceanogr.*, **23**, 1346–1362.

Wiin-Nielsen, A., 1967: On baroclinic instability as a function of the vertical profile of the zonal wind. *Mon. Wea. Rev.*, **95**, 733–739.

Williams, G.P., 1978: Planetary circulations: 1. Barotropic representation of jovian and terrestrial turbulence. *J. Atmos. Sci.*, **35**, 1399–1426.

———, 1979a: Planetary circulations: 2. The jovian quasi-geostrophic regime. *J. Atmos. Sci.*, **36**, 932–968.

———, 1979b: Planetary circulations: 3. The terrestrial quasi-geostrophic regime. *J. Atmos. Sci.*, **36**, 1409–1435.

———, 1988: The dynamical range of global circulations—I. *Clim. Dyn.*, **2**, 205–260.

———, 1996: Jovian dynamics. Part I: Vortex stability, structure, and genesis. *J. Atmos. Sci.*, **53**, 2685–2734.

———, 2002: Jovian dynamics. Part II: The genesis and equilibration of vortex sets. *J. Atmos. Sci.*, **59**, 1356–1370.

———, 2003a: Jovian dynamics. Part III: Multiple, migrating, and equatorial jets. *J. Atmos. Sci.*, **60**, 1270–1296.

———, 2003b: Barotropic instability and equatorial superrotation. *J. Atmos. Sci.*, **60**, (in Press).

——— and R.J. Wilson, 1988: The stability and genesis of Rossby vortices. *J. Atmos. Sci.*, **45**, 207–241.